TRANSIT TIME FLOW METER APPLICATION TO CLOSED PIPES DEMANDING HIGH ACCURACY

A DISSERTATION

Submitted in partial fulfilment of the requirements for the award of the degree of

MASTER OF TECHNOLOGY

in

ELECTRICAL ENGINEERING

(With Specialization in Measurement & Instrumentation)

By

PREM VASANTHA KUMAR MANDIMALA

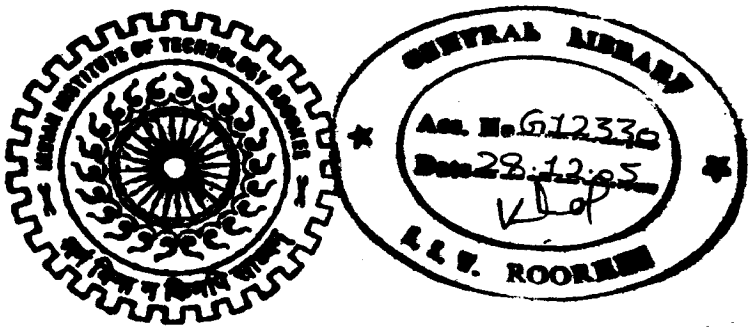

DEPARTMENT OF ELECTRICAL ENGINEERING
INDIAN INSTITUTE OF TECHNOLOGY ROORKEE
ROORKEE-247 667 (INDIA)

JUNE, 2005

CANDIDATE'S DECLARATION

I hereby declare that the work that is being presented in this dissertation report entitled **"TRANSIT TIME FLOW METER APPLICATION TO CLOSED PIPES DEMANDING HIGH ACCURACY"** submitted in partial fulfillment of the requirements for the award of the degree of **Master of Technology** with specialization in **MEASUREMENT AND INSTRUMENTATION,** to the **Department of Electrical Engineering, Indian Institute of Technology, Roorkee,** is an authentic record of my own work carried out, under the guidance of **Dr. H. K. VERMA,** Professor, Department of Electrical Engineering and **SHRI ARUN KUMAR,** Head and Chief Scientific Officer, Alternate Hydro Energy Centre.

The matter embodied in this dissertation report has not been submitted by me for the award of any other degree or diploma.

Date: 28th June '05

Place: Roorkee

(PREM VASANTHA KUMAR MANDIMALA)

This is to certify that the above statement made by the candidate is correct to the best of my knowledge.

28/6/05

Dr. H. K. VERMA
Professor,
Department of Electrical Engineering,
Indian Institute of Technology Roorkee,
Uttaranchel - 247 667, INDIA.

ARUN KUMAR
Head and CSO,
Alternate Hydro Energy Centre
Indian Institute of Technology Roorkee
Uttaranchel - 247 667, INDIA.

ACKNOWLEDGEMENT

I am very indebted to my institution, **Indian Institute of Technology, Roorkee** for providing me opportunity to pursue my Masters. The lessons that this campus has taught are of immense value to me and I hope to cherish over the memories of this stay in the years to come.

Thanks to Head, Department of Electrical Engineering, Group leader and the team of **MEASUREMENT AND INSTRUMENTATION** for extending their co-operation in the academic proceedings.

Dr. H. K. VERMA, Professor, Department of Electrical Engineering, IIT Roorkee, my guide is the first person behind the success of this dissertation. "*Great men are as gentle as flowers and as strong as trees*", that is my guide. I frankly admit that this work evolved through substantial discussions with him. He was my motivation all through the work and had been a great encouragement at times when I stuck up. Man of his own kind, I salute to his perfection. For sure, learning under him is a unique experience.

I should be grateful to **SHRI ARUN KUMAR,** Head, Alternate Hydro-Energy Company, IIT Roorkee for giving me an opportunity to work in Hydraulics Lab, AHEC. I am very much an admirer of his enthusiasm and mingling nature. He has been a knowledge resource to me through out the work.

I thank **PROF. THOMAS STAUBLI,** HTA LUZERN, for his prompt suggestions and insights furnished to me during his visits to India and thereafter.

I thank the personnel at Central Library, IIT Roorkee for maintaining a good collection of online journals, I wish that the subscriptions are extended to diversified fields of research.

I am left indebted to all my friends, for letting their lives run beside mine for a while. They had always been a cheerful company to me. My gratitude to them cannot be expressed in words, i thank all my friends for rendering a ready help whenever I needed.

In the first place, I thank my God and my family for all that they are to me. I humbly dedicate this thesis work to my ***DAD.***

"WE ARE MERELY PICKING UP PEBBLES ON THE BEACH, WHILE THE GREAT OCEAN OF TRUTH LIES UNDISCOVERED BEFORE US."

- SIR ISAAC NEWTON

ABSTRACT

Discharge (flow rate) measurement in hydro-power station is one complex measurement application which demands very accurate methods. For years together the accuracy of flow measurement remained unsatisfying, until the high speed digital age took over the analog methods. Latest state of art technologies like the high speed signal processing and the smart sensor design being used in the application of ultrasonic transit time flow meter for discharge measurement improved the accuracy to a good extent. The promised accuracy using an eight-path ultrasonic transit time flow meter is ±2%.

The complexity of fluid dynamics with respect to closed pipe flow influences the measurement of discharge. Though various correction methods have been tried over the past 20 years, yet the accuracy demands have not been met. Various errors associated with the application of ultrasonic transit time flow meter to closed pipes are Reynolds number error, surface roughness error, installation and survey errors, protrusion effect, roundness effect and the *numerical integration error*. The focus of this dissertation work is to improve the accuracy of the ultrasonic transit time flow meter applied to closed pipes by minimizing the numerical integration error, which influences the accuracy of flow measurement significantly.

The mathematical expressions of velocity profiles in combination with the finite element analysis techniques have been used to study the numerical integration error as influenced by the kind of profile and the numerical integration method used. These findings formed the basis of applying artificial intelligence techniques to minimize numerical integration error. A neuro-fuzzy model is designed to work for the discharge measurement using transit time ultrasonic flow meter. The model yields a zero error for known profiles and restricted the numerical integration error for new profiles to an as low as 0.5 %.

LIST OF FIGURES

LIST OF TABLES

CONTENTS

CHAPTER 1

INTRODUCTION

The discharge measurement in a closed pipe is a complex phenomenon. There are several methods being employed for measuring the discharge in closed pipe like current meter, electromagnetic, ultrasonic transit time, tracer methods and thermodynamic. Due to rather relative achievement in greater accuracy and being promising for discharge measurement, the UTTF has been the subject of this study.

1.1 ULTRASONIC TRANSIT TIME FLOW METER (UTTF)

Ultrasonic transit time flowmeter (UTTF) is one of the modern instruments that uses the state of art technologies. The speed of digital signal processing combined with the floating point processors made the UTTF a reality. Today UTTF is one of the widely used techniques in determining the flow rate with highest accuracies.

Though measuring flow using the transit time technique is known for over sixty years, yet its commercial success is seen in recent years owing to problems related to instrumentation. Measuring flow using UTTF promises good accuracy (less than ± 2 %). The application of UTTF to closed pipes for discharge measurement in hydro-power stations is dealt with in the dissertation. An attempt to improve the 'as obtained' accuracy of the UTTF is made. The objective of the work is to limit the in accuracy of UTTF due to numerical integration to within $\pm 0.5\%$.

Accuracy improvement of any instrument starts from the point of identifying the sources of errors. Next step is to find out how these errors can be minimized. Correction of these errors is always a practical tradeoff between cost and the accuracy demanded.

Correction of an error in a way can be alteration in the hardware of the meter. Developments in the interfacing technology enabled instruments to talk to computing machines. Various interfaces like USB, serial link and GPIB act as connectors between

instruments and PC /Laptop. Thus errors can also be corrected through interfacing software, which is feasible, quicker and an economical way of error correction.

There are two basic types of UTTFs classified by the kind of transducers they use. The first type is called 'clamp-on meters' which are installed on the pipe's outer surface while discharge is measured. The accuracy of measurement by clamp-on meters is subject to the variation of the speed of ultrasonic waves in the pipe material and the refraction effects. The second type are the ones which use the wet transducers. These are very accurate as they directly come in contact with the flow conduit, thus recording the flow velocity as accurately as possible. The eight-path UTTF that uses wet transducers is taken up for accuracy improvement.

The primary objective of this work is to improve the meter performance for discharge measurement. The emphasis is laid on application of UTTF for discharge measurement to closed pipes in hydro-power stations.

1.2 APPLICATION OF UTTF TO CLOSED PIPES

Standardization of UTTF application to closed pipes for discharge measurement can be found in internationally accepted International Electromechanical Commission, (IEC) standard number 60041, which declares the code to be followed for discharge measurement in hydro power station [1]. Though the classical transit time flow meters are designed with a single path comprising of two transceivers talking to each other, research in this area proved that accuracy of meter increases as number of paths are increased. IEC 60041 suggests an eight path UTTF that promises accuracy less than 2 %.

Unlike open channels, pipes are closed, and installation of the flow meter will be an issue of importance. The first step in measurement of discharge in closed pipes involves choosing the measurement section, which should be followed by insertion of transducers at precise positions specified by IEC 60041. The instrument takes care of computation of transit times of individual paths and display of the discharge.

1.3 FLOW MEASUREMENT IN HYDRO POWER STATIONS

Measuring flow rate (discharge) is one of the vital parameters in determining efficiency of hydroelectric turbines. The other parameters appearing in the efficiency measurement are the water head and the electric output of the hydroelectric generating unit, both of which can be determined with good accuracy without much difficulty. Therefore the accuracy of efficiency measurement is largely decided by the accuracy of flow measurement.

The main issue that needs attention when UTTF is employed for discharge measurement in hydro-power stations is 'measurement section'. Not all hydro-power stations have measurement section as specified IEC 60041, which in turn suggests us that the accuracy is effected by different deviations from the code specified as per IEC 60041. Analytical presentation of such deviations of measurement section is also addressed in the dissertation work.

1.4 OBJECTIVES OF DISSERTATION

The following are the objectives of dissertation work briefly stated:

- Identify the sources of error while applying UTTF to closed pipes in hydro-power stations.
- Obtain the correction factors for the identified sources of error.
- Design a model of UTTF accordingly and check for accuracy improvement.

1.5 ORGANIZATION OF DISSERTATION REPORT

The dissertation report is organized as follows:

Chapters 1 and 2 introduce the dissertation work and ultrasonic transit time flow meter respectively.

Chapter 3 is devoted to describe the complexity of pipe flow with an introduction to the fully developed turbulent flow.

Chapter 4 introduces the various sources of error, with a perspective toward the correction of the errors specified.

Chapter 5 describes three numerical integration methods namely Gauss-Jacobi, Gauss-Legendre and Optimal weighted integration for closed sections, with respect to the numerical integration error.

Chapter 6 discusses the origin and behavior of flow profiles with the variation in the parameters of analytical expressions, these were used as database for finite element analysis and further extension of the work.

Chapter 7 presents the results of the finite element analysis of the three numerical integration methods under discussion and the variation of numerical integration error for each of the 14 profiles taken up.

Chapter 8 presents the results of the neuro-fuzzy model designed for the profile recognition and discharge prediction.

Finally, chapter 9 concludes the report putting forth the scope of further work that can be done as an extension of this dissertation work.

CHAPTER 2

ULTRASONIC TRANSIT TIME FLOWMETER

2.1 THEORY AND BACKGROUND

Primitive single path UTTF consists of two transceivers, which are mounted on either side of the flow conduit, and at an angle to the flow direction. An ultrasonic wave is exchanged between the two transducers. The time difference between the upstream time and downstream time is called the transit time. Transit time is directly proportional to the flow rate in the conduit. The circuit on which the UTTF works is illustrated in Fig.2.1

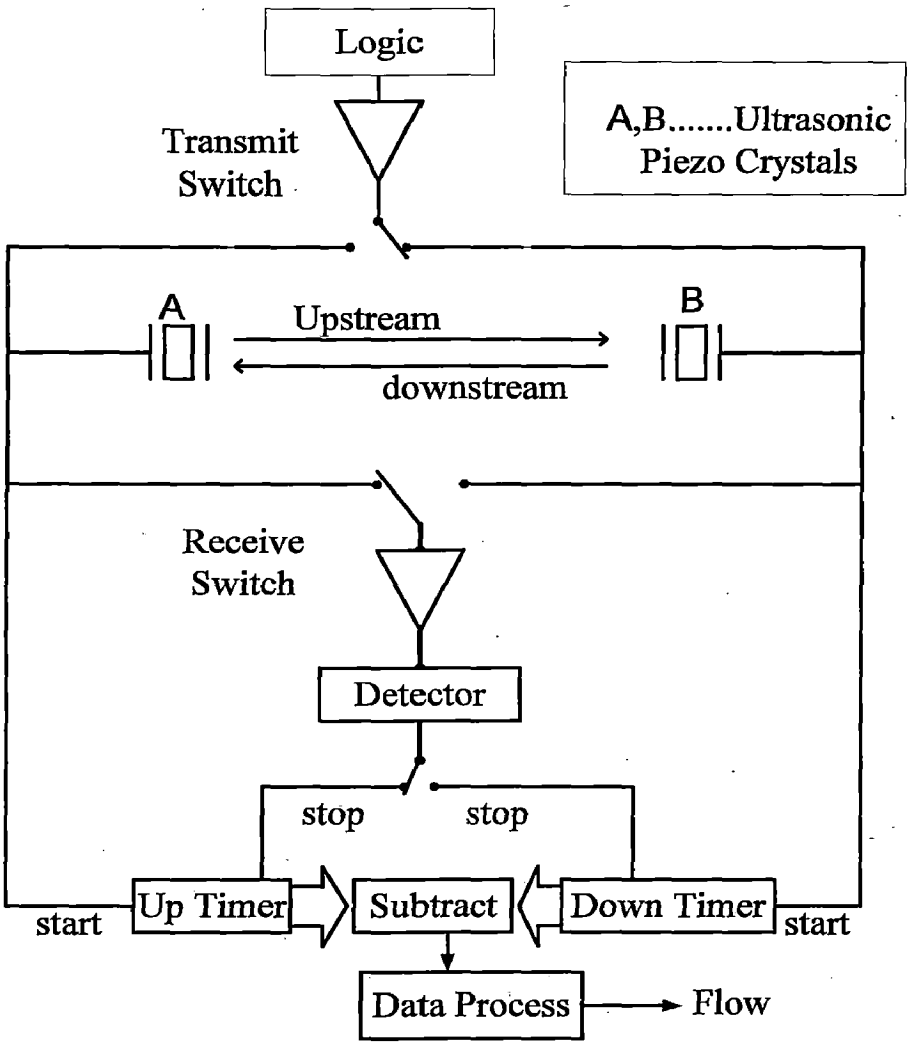

Fig.2.1 Basic circuit of single path UTTF.

The governing equation for mean flow calculation using single path UTTF is as follows:

$$\overline{V}_{ax} = K\frac{L}{2.\cos\alpha}.\left(\frac{1}{t_d} - \frac{1}{t_u}\right) \tag{2.1}$$

where

t_u is the upstream time,

t_u is the downstream time,

L is the length of the ultrasonic path,

α is the angle made by the ultrasonic path with the flow direction,

$\overline{V}_{ax}$ is the average flow velocity measured along the ultrasonic path and

K is the shape factor.

For pipe diameter of 150 mm at a 60 degree angle of the ultrasonic path with the flow direction with a flow velocity of 1 m/s at water temperature of 20 degree, the transit times of about 116 s and a transit time difference on the order of 79 ns [2].

Flow rate in the conduit is not uniform but is subject to the shape of the conduit, Reynolds number, conduit roughness and transducer protrusion etc. The mean flow rate of flow conduit is the average value of the flow velocity sampled over the cross section of the flow conduit. The accuracy of flow rate calculation is proportional to the area of interrogation of the flow conduit. Reynolds number for the flow in hydro-power stations is a high (typically 4×10^5 to 3×10^6), which implies that it is a turbulent flow. Thus the flow distribution is not only non-uniform but also contains the transverse component in it.

A single path UTTF measures average flow velocity along the ultrasonic path. The diametrical path flowmeter is more sensitive to the flow distribution in the conduit. The mid radius path UTTF combined with correction factor (as function of Reynolds number) is observed to show better accuracy than the diametrical path UTTF [3]. With the intension of making a better interrogation of the flow conduit, the number of ultrasonic paths was increased to two. Individual path velocities are integrated by numerical integration techniques. This gave the two-path UTTF to have control on the estimation of

flow rate as function of flow velocity confined between the two ultrasonic paths. A four path UTTF was observed to perform better than the two path flowmeter. Fig. 2.2 illustrates the single path, double path and four-path UTTF.

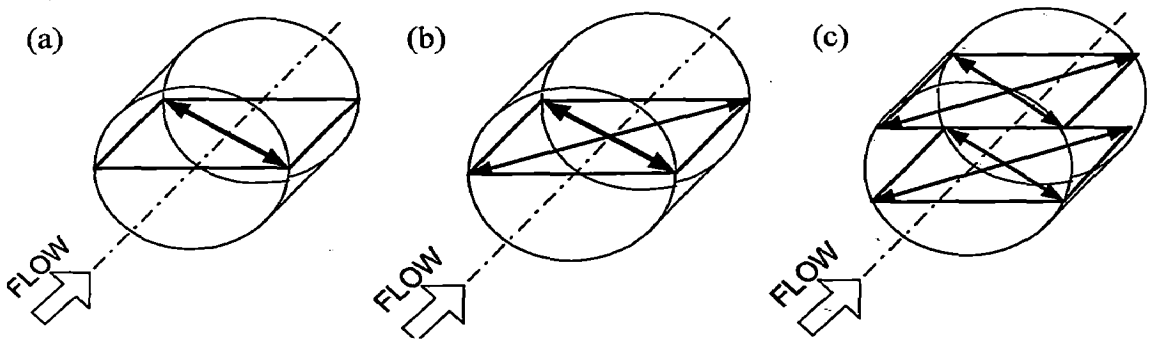

Fig. 2.2 (a) Single path UTTF.
(b) Double path UTTF.
(c) Four path UTTF.

The accuracy of flow rate measurement increases with the increase in the number of paths. But on adding an ultrasonic path, the cost of the transducers and the installation cost are to be added. IEC 60041 proposes an eight path UTTF for discharge measurement as a tradeoff between accuracy and cost. IEC 60041 promises accuracy of 2 % in discharge measurement but only under certain conditions that must be satisfied by the field situation. The eight path ultrasonic flowmeter cancels out the transverse component in the flow, but accounts least for asymmetric nature of flow distribution. A comprehensive description of application of UTTF to discharge measurement and working of UTTF can be found in [4].

2.2 EIGHT PATH UTTF: A CRITICAL EXAMINATION

The eight path UTTF suggested by IEC 60041 is such an application for flow measurement, which involves many instructions that has to be strictly followed. The section where the ultrasonic transducers are installed is called the measurement section. One important rule is that the 'measuring section' should have a straight conduit of 10 diameters upstream and 3 diameters downstream. It is difficult to fulfill this condition due to topology of the hydro-power station, and especially in small hydro-power stations.

An eight-path UTTF has two ultrasonic paths in a plane and four such planes distributed over the whole cross section of the conduit. The transverse component of the flow is compensated by the axis-symmetric path in a plane. But still the measurement can be made by the four horizontal paths installed in vertical pane, provided that the flow is free from transverse components. The discharge measurements made this way are found to be satisfactory in many instances. So not necessarily eight-path UTTF be used to make the discharge measurement if the knowledge of how intense is the influence of the transverse component is available. Transverse flow component is influenced by the disturbances such as valves and obstacles in the upstream conduit in the proximity of measuring section.

The Gaussian numerical integration methods are suggested by [1] for the eight-path UTTF. But both of the Gaussian quadrature techniques namely, Gauss-Lacobi and Gauss-Legendre are very well suited for smooth flow distribution in the conduit. The methods doesn't account for steep variations in the flow profile, which results in error typically less than 0.5 to 1 % . The need of better technique that can very well reduce this error is met by Optimal Weighted Integration for Circular Sections (OWICS) [5]. The performance of OWICS was recognized and was adopted by few manufacturers of UTTF [6]. A further discussion on OWICS is presented in 5th chapter. A typical setup of an 8-path UTTF is shown in following figure:

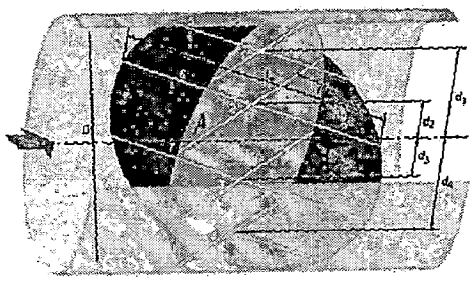

Fig. 2.3 An eight path UTTF
(Source: technical data sheets of Risonic 2000, Rittmeyer)

IEC 60041 suggests weighting factors for the two Gaussian quadrature techniques and the correction factors depending on the shape of the conduit. The weighting factors and the parameters that are used in the discharge calculation of the discharge by an eight-path UTTF are reproduced in Table 2.1.

Table 2.1. Weighting coefficients for discharge measurement using eight-path UTTF

		Gauss-Legendre method		Gauss-Jacobi method	
		Paths 1 and 4	Paths 2 and 3	Paths 1 and 4	Paths 2 and 3
d/(D/2)		± 0.861136	± 0. 339981	± 0.809017	± 0.309017
W		0.347855	0.652145	0.369317	0.597667
k	Circular section	0.994		1	
	Rectangular section	1		1.034	

The error due to installation and the complexity of near wall flow are not much accounted by IEC 60041. Further improvement in the promised accuracy (2 %) of the UTTF is possible if the two above mentioned problems are dealt with appropriating. The expression used for discharge calculation using multi-path UTTF is given below.

$$Q = k\frac{D}{2}\sum_{1}^{n} W_i \bar{v}_{ai} L_{wi} \sin\varphi \qquad (2.2)$$

where

φ is the angle made by the i^{th} path with flow direction,

L_{wi} is the distance from pipe wall to pipe wall along the i^{th} ultrasonic path,

$\bar{v}_{ai}$ is the flow velocity averaged along i^{th} path,

W_i is the weighting factor of i^{th} path depending on the numerical integration method used,

n is the number of UTTF paths,

D is the diameter of the pipe,

k is the correction factor depending on the numerical integration method and the shape of the conduit and

Q is the discharge measured.

CHAPTER 3

COMPLEXITY OF PIPE FLOW

The headrace of a hydro-power station is called penstock that carries the hydraulic force on to the turbine. The penstock in most cases is a circular section, more precisely a pipe. The advantage of penstock being a pipe or circular section is that the momentum due to head can be effectively transferred to the turbine, reducing the losses. The basic question is of 'how can be the flow distribution in a pipe be defined?'. Investigation by various research workers on pipe flow has contributed to the present status of the pipe flow.

The primitive research workers (*Poiseuillie, Hagen and Nuemann*) on pipe flow analysis put forth a laminar flow definition. The flow was considered as a series of cylinders which slide over each other as the flow proceeds through the pipe. Fig. 3.1. illustrates the description equation given by (3.1).

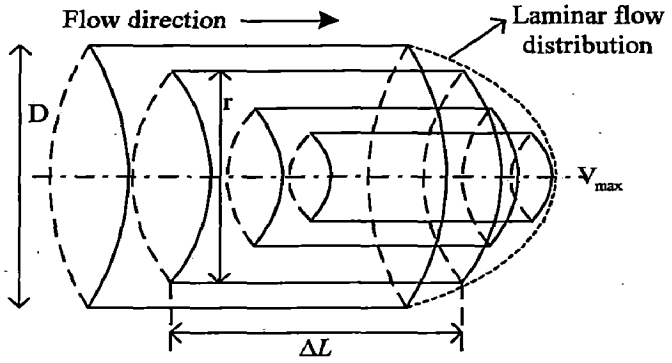

Fig. 3.1. Poiseuille's view of laminar flow in pipe

$$v = -\frac{\Delta P}{\Delta L}\frac{1}{4\mu}\left(\frac{D^2}{4} - r^2\right) \tag{3.1}$$

where

r is the radius of the hypothetical cylinder,

D is the diameter of the pipe,

μ is the dynamic viscosity,

ΔP is the viscous resistance (assumed to be uniform),

ΔL is the length of the hypothetical cylinder and

v is the velocity at point r in the pipe.

3.1 REYNOLDS NUMBER

It was *Osborne Reynolds's* classic dye experiment at Manchester university that brought into light that flow profile is not always laminar, but is function of the some parameter [7]. The parameter that was proposed is 'Reynolds number' after his name. in the subsequent years and till date Reynolds number has been an important parameter of pipe flow analysis and definition. Equation 3.2 defines Reynolds number.

$$R_e = \left[\frac{a\bar{v}}{\nu}\right] \qquad (3.2)$$

a is linear dimension

where

$\bar{v}$ mean velocity measured in the conduit,

ν kinematic viscosity,

a the area of cross section of the conduit and

R_e is the Reynolds number.

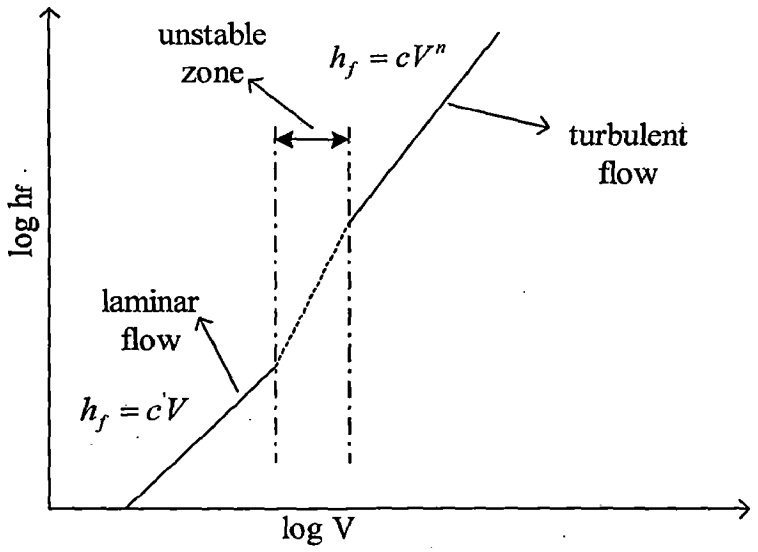

Fig 3.2. Three flow zones.

The Reynolds number defines the nature of the flow. The flow is considered 'laminar' if the R_e is approximately less than 2300 and is termed as 'turbulent' if the R_e is above 4000. The nature of flow for R_e falling between 2300 and 4000 is neither laminar nor turbulent but is hybrid of the two characteristics. This zone is termed as unstable zone.

termed as unstable zone. Moreover the zone is not sharply defined. Fig. 3.2 shows the variation between head loss, h_f and the mean flow velocity, V, in a pipe illustrates the above description clearly. In the laminar region the head loss is directly proportional to the flow velocity, while in the turbulent region the losses are still high due to the eddy motion of the fluid particles.

3.2 FRICTION FACTOR AND LAMINAR SUB-LAYER

While head losses still remained as the focus of the research on pipe flow analysis. The introduction of Reynolds number has paved a way to define the friction factor of the pipe as function of R_e. *Blasius* is the first among researchers who put forth a relation between the friction factor and R_e. The relation was purely based on the pipe friction data supplied by *Saph* and *Schoder*. *Blasius's* inferences were straight forward. Incase of smooth pipes the friction factor is only dependent on R_e, while incase of rough pipes the friction factor is a function of the R_e and relative roughness. The relative roughness is ratio of the roughness of the inner pipe wall to the inner diameter of the pipe. The equation formulated by *Blasius* is as follows:

$$\lambda = \left[\frac{0.316}{R_e}\right] \tag{3.3}$$

where λ is the friction factor.

The actual verification of *Blasius's* inferences is done by *Nikuradse* [8]. The friction data for Reynolds numbers ranging from the laminar zone to turbulent zone are obtained. The contribution of *Nikuradse* to friction factor in rough pipes was substantial. But roughness was created artificially in the lab, by evenly fastening sand grains uniformly over the internal surface of the pipe. In view of this the semi-empirical relations obtained by him did not account for height, pattern and spacing between the excrescences. Smooth curves are plotted between friction factor and R_e for different values of relative roughness, k/D, where k is the roughness height and D is the diameter of the pipe. The results raised up three important conclusions which are as follows:

(a) In laminar region the friction factor is independent of the degree of roughness.
(b) In turbulent region (R_e>4000) the friction factor followed certain fashion with Reynolds number.
(c) Simple empirical relations of friction factor and Reynolds number holds well only within limited ranges (so the graph is more like a piece-wise function than being continuous).

One clear observation that was made from *Nikuradse's* work is that the flow nature in the transitional region is very unpredictable. The graphs plotted did not show any trend in the transitional region. More interesting excerpt from *Nikuradse's* work is the 'laminar sub-layer'. The flow near the pipe inner wall is subject to the drag forces of the excrescences of the pipe wall, thus resulting in a very low or almost zero flow velocity near the flow. The Reynolds number corresponding to the flow velocities near the wall reveal that it is laminar. The next stage of the flow is the transitional region through which the laminar flow changes to a completely turbulent flow. This transitional region which is very thin, in comparison with the diameter of the pipe is called the 'laminar sub-layer'. The laminar sub-layer has been for many years, a much focused topic of research and is the same till today. Owing to its thinness, investigation into the laminar sub-layer is limited.

The transitional formula for 'laminar sub-layer' is put forth by two researchers at Imperial College, namely *Colebrook and White* [9]. Separate empirical relations of friction factor for laminar flow and the turbulent flow are combined to result in single 'transitional formula'. The transitional formula joined the discontinuities of *Nikuradse's* curves to make them continuous over the whole practical range of Reynolds number. But in no way the transitional formula is said to be exact, though the formula validates itself with the experimental facts. Because experimental constants rather than empirical are necessary for the practical application of the formula. More insights on the friction factor analysis can be found along with generalization on the friction and roughness constants for different commercial pipes can be found in [8, 9, 10].

3.1 FULLY DEVELOPED FLOW

The flow in closed conduits (especially pipe) if allowed to travel in straight paths over long distances in comparison to the diameter of the pipe, then the flow profile achieves equilibrium, the flow profile retains such stable definition even if it is allowed to traverse further through straight pipe. Such a stable definition is called the 'fully developed flow' [11]. The fully developed flow is mostly turbulent in nature. The flow distribution is almost smooth and symmetric in nature. It is very important for the flow profile to achieve such a state of 'fully developed flow' before reaching the measuring section, which otherwise will contribute to errors due to unpredictable distorted flow profile.

The 'fully developed flow' can be mathematically described by power law function. But unlike the laminar flow which is defined by the parabola, a power law with an exponent of two, the 'fully developed flow' is can be best described by exponent, '1/n' which varies from 1/9 to 1/7. 'n' depends on the Reynolds number of the flow and the roughness of the pipe. The flow profile stays smooth all over the cross sectional area, but on reaching the wall of the pipe the profile cuts steep along the wall of the pipe reaching almost zero velocities.

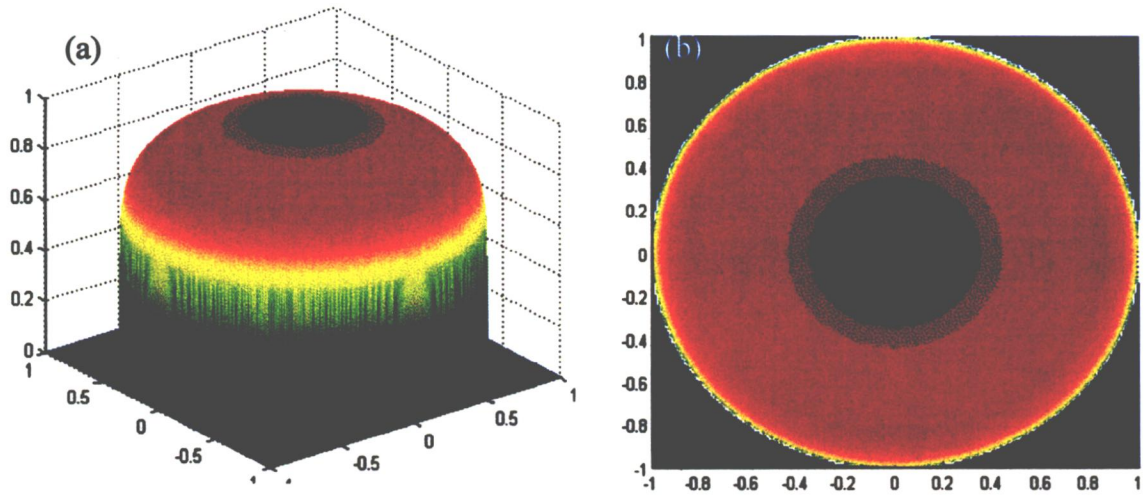

Fig. 3.3. Fully developed flow. (a) 3D view of the flow profile (b) 2D projection of the same on the cross-section of the pipe.

The power law that for illustrated flow profile of a typical fully developed flow can be given by the following equation:

$$V(r) = (1 - r)^{1/n} \tag{3.4}$$

where

r is the normalized radius,

n is the exponent in this case n=9 and

V(r) is the flow velocity of a point at a distance r from the axis of the pipe.

Proceeding from the wall to the axis of the pipe, the flow velocities near the wall is almost zero, due to the drag forces of the excrescences on the pipe inner surface. The near-wall flow is laminar in nature. The laminar region then opens into a smooth turbulent region through a very thin transition region. Fig. 3.3. shows a typical fully developed flow in a pipe. Primary question in pipe flow analysis is the definition of the near-wall flow. The flow in the penstock of hydro–power stations is turbulent, which means that the flow profile is not always a uniform or symmetric kind. It gets distorted by the bends, tapers and discontinuities in the penstock. Proceeding from the wall toward the centre of the pipe, the flow changes from laminar to turbulent through a very thin transition region (laminar sub-layer). The transition region opens into a smooth turbulent core, which extends till the axis of the pipe and most likely the maximum flow velocity is at the centre of the pipe.

The complexity of the flow is neither the near-wall laminar flow nor the smooth turbulent core, but the transition region.

CHAPTER 4
SOURCES OF ERROR: CORRECTION PERSPECTIVE

No measurement is free from error, so was the discharge measurement with UTTF. Discharge measurement with an eight-path UTTF is an application that has to account for many factors related to the fields of fluid mechanics, civil engineering, electrical, electronics and instrumentation. IEC 60041 specifies 8 instrument errors and 4 systematic errors. Among these, few errors were identified to largely influence accuracy of the UTTF. Those errors give scope to correct the "as obtained" accuracy and are listed as follows:

1. Reynolds number error
2. Roughness error
3. Installation and survey errors
4. Error due to protrusion effect
5. Roundness error
6. Numerical integration error (etc.)

The first step to deal with the errors is to establish a relationship between the parameter responsible for the error and the error in discharge measurement. The next step is to account for them through 'compensation' or with an error correction factor, so that the accuracy of UTTF is improved. The errors are discussed in brief in the following sections. The correction can be an enhancement or modification in the hardware of the instrument or a novel in approach of measuring the discharge. Connectivity of the instruments to the computer has enabled improvement in accuracy in a more economical way. The accuracy can be improved by a 'correction factor' supplied through a software package that can deal with the discharge measurement on real time basis. The packages like visual studio, Matlab and LabVIEW can be used as platforms for connectivity to the instrument.

4.1 REYNOLDS NUMBER ERROR

The Reynolds number is the basic parameter underlying, which influences the nature of flow profile. Direct consequences of the Reynolds number on flow measurement can be

observed in a single path UTTF. Where the flow velocity measured by the single path and the mean flow rate of the whole cross section of the conduit are related through a function in Reynolds number (R_e).

$$\frac{\text{Mean flow measured}}{\text{Path flow measured}} = f(R_e) \tag{4.1}$$

$$\overline{V} = V_{max}(1+0.19R_e^{-0.1}) \tag{4.2a}$$

$$\overline{V} = V_{max}(1+0.01\sqrt{6.15+431R_e^{-0.237}}) \tag{4.2b}$$

where

$\overline{V}$ is the flow velocity measured by the ultrasonic path and

V_{max} is the maximum velocity of the turbulent flow profile.

Empirical relations can be obtained from [2, 12, 13] and are given in Eqns. (4.2a) and (4.2b). The error was understood more as an influence of Reynolds number on the measurement path than on the flow profile. The correction of the Reynolds number is significant, due to the reason that the flow is no more of single kind, but is complex, a mixture of 3 different kinds of flow corresponding to different ranges of Reynolds numbers across the pipe cross section.

The Reynolds number correction for a multi-path UTTF can be applied separately to each path, individual path velocities can be corrected before them being used in discharge calculation.

4.2 ROUGHNESS ERROR

The roughness error correction is another challenging task. The parameter of significance in this case is the roughness height 'k_s' that can be measured with techniques such as Laser Doppler anemometer. Moreover an important deduction is that roughness error is also influenced by the diameter of the pipe, so a relative parameter, 'k_s/D' is taken into account for the roughness error correction. The experimental analysis of influence of roughness parameter on mean flow rate in commercial pipes can be found in [8, 9]. The

friction factor λ is standard parameter used to express the value of k_s. The primitive relationship between λ and k_s, put forth by *Colebrook and White* can be found in [9]. The friction factor is dependent on the function of R_e, the corresponding value of R_e for given friction factor can be found out by standard λ-R_e diagram.

An indirect study of influence of roughness on mean velocity can be made by calculating the head loss for different relative roughness in pipes over a known distance of flow conduit. One such experimental observation was made in [14]. The head loss and the friction factor are related through an empirical relation, but a generalization on this is yet to be achieved. Three different formulae are proposed to deal with smooth, transition and rough pipes. Manning's formula, which is generally applied to open channels, can be interpreted to closed pipes. An inference from Manning's formula is given as follows:

$$\lambda = \frac{n^2}{D^{1/3}} \tag{4.3a}$$

$$n = \frac{D^{1/6}}{22.3\log(3.7D/k_s)} \tag{4.3b}$$

where

λ is the friction factor,

D is the diameter of the pipe,

k_s is the roughness height on the inner wall of the pipes and

n is the integer based on the value of k_s and D.

The Manning's formula is simpler empirical relationship that proved to be better than others. The friction factor can be used to apply the correction for the velocity depending on the behavior of the velocity profile with the variation in the roughness of the pipe. The nature of pipes as smooth, transition or rough can be judged from the *Nakuradse's* work, in which the formula for the thickness of 'laminar sub-layer', δ_L is derived. The expression is as follows:

$$\frac{\delta_L}{D} = \frac{32.8}{R\sqrt{\lambda}} \tag{4.4}$$

Excrescences of the pipes are compared against the calculated value of δ_L, accordingly the classification of the pipes into the three sections is carried out. Fig 4.1 illustrates a pictorial comparison.

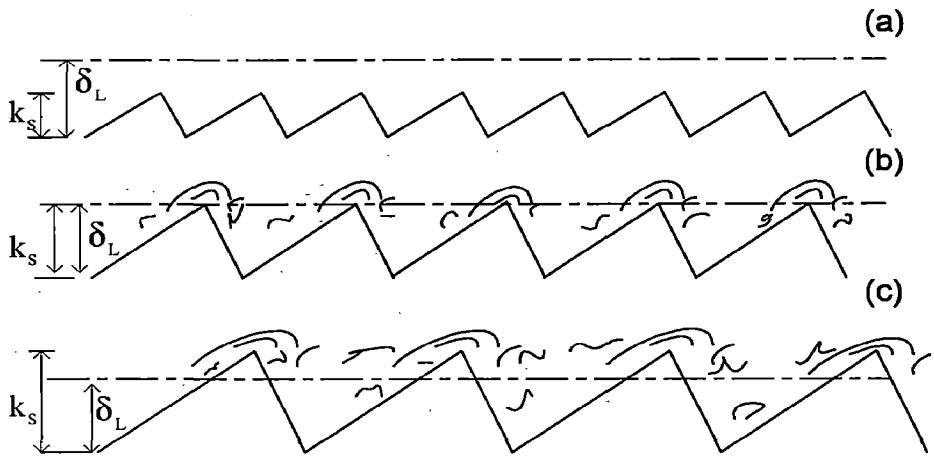

Fig 4.1. Excrescences on the pipe inner wall

(a) smooth pipe, $k_s < \delta_L$

(b) Transitional pipe, $k_s \sim = \delta_L$

(c) Rough pipe $k_s > \delta_L$.

The roughness error increases with the increase in the roughness height and decreases with the increase in the diameter of the pipe. Friction factor analysis also gives friction factor as a function of Reynolds number [15]. More recent work on relationship of friction factor from direct measurements of roughness of the pipe can be found in [16], but for the experimental verification was carried out for UTTF applied to natural gas flow.

4.3 INSTALLATION AND SURVEY ERRORS

The accuracy of the mounting transducers is largely dependent on the measurement of diameter, path length and installation angle. The measurement of diameter is an important factor in deciding the path lengths of the UTTF, path angle, etc. IEC 60041 suggests the measurement of diameter as an average from five points evenly distributed across the

measuring section. But the lateral distances at which the ultrasonic paths have to be mounted is of six digit precision after the decimal point (Table 2.1). A surveying instrument called 3D Theodalite is capable of measuring distances with such a precision is used while installing ultrasonic paths [17]. A numerical integration technique as an error correction against the installation error, is presented in [18]. This technique termed as Optimal Weighted Integration for Circular Sections (OWICS), calculates the weighting factors from the actual lateral distances at which the paths are installed other than those specified in IEC 60041. The method seems to take care of the integration error in the near wall flow of fully developed flow to some extent.

The results for distorted profiles, which are presented in [18] show that the OWICS had outperformed Gauss-Jacobi numerical integration method by an improvement in error approximately of 1.5 %, but the precision remained the same.

4.4 PROTRUSION EFFECT

The UTTF can be applied to measure discharge using two kinds of transducers, namely wet and clamp-on transducers. Clamp-on transducers as the name implies stand outside the pipe and measure the flow velocity, while wet transducers come in direct contact with the flow conduit. Owing to the significant error in calculation of transit time due to refraction of the ultrasonic ray through the pipe material, the clamp-on meters are not standardized for applications demanding high accuracy. The wet transducers have performed better in comparison with the clamp-on kind.

But the one immune effect of wet transducers is that, it induces distortion in the sensitive region (transition region) of the flow profile. The major issues that are to be discussed with respect to the protrusion of the transducer into the flow conduit are as follows:

- Sampling error – some part of the flow profile is left un-sampled by the ultrasonic

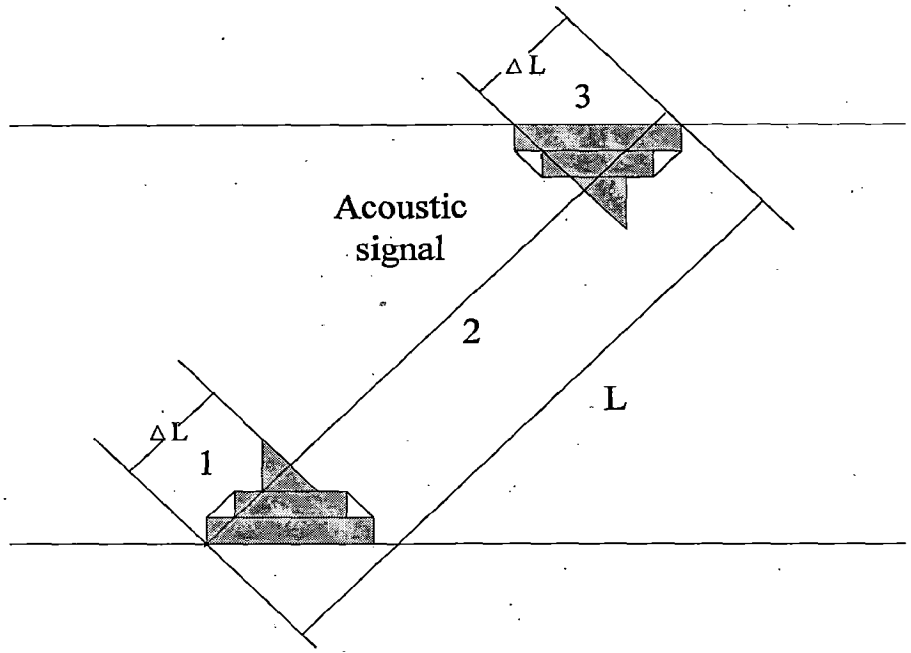

Fig. 4.2. Protrusion effect (side view of the conduit)

CFD simulation of the transducer protrusion puts forth a method of correction against the protrusion effect for discharge measurement [19]. The effective path length for each of the UTTF paths is length of the line joining the two transducer ends, where the ultrasonic wave emanates. Each UTTF path can be divided into 3 sections proceeding from one transducer along the path to the other transducer. Section 2 (Fig. 4.2) is free from the influence of the protrusion. Sections 1 and 3 are influenced by protrusion and needs correction for the same. The influence of the protrusion is ratio between flow velocity with and without protrusion, which is called the protrusion coefficient, f.

$$f = \left[\frac{\int_0^{l_{oD}} V'_{Proj}(s)ds}{\int_0^{l_{oD}} V_{Proj}(s)ds} \right] \tag{4.6a}$$

$$\overline{V_i} = \left[\frac{f_i \int_0^{l'_{iD}} V_{Turb}(s)ds + \int_{l'_{iD}}^{l_i - l'_{iD}} V_{Turb}(s)ds + f_i \int_{l_i - l'_{iD}}^{l_i} V_{Turb}(s)ds}{l_i} \right] \tag{4.6b}$$

where

$V'_{Proj}(s)$ is the projected velocity with protrusion,

$V_{Proj}(s)$ is the projected velocity without protrusion,

f_i is the protrusion coefficient of the transducers installed along the inner UTTF paths,

$V_{Turb}(s)$ is the velocity in a fully developed turbulent flow,

L_i is the effective length and

V_i is the mean flow velocity in regard to protrusion effect.

Equations (4.6a) and (4.6b) provide with expressions for the flow velocity calculation incase of protrusion. Important conclusions that can be reached on protrusion are:

- The effect of protrusion decreases linearly with the increase in the diameter of the pipe.
- The upstream transducer influenced the discharge measurement non-linearly compared to the downstream transducer.

4.5 ROUNDNESS ERROR

The construction of large diameter pipes which are generally found in hydro-power stations is not perfectly circular. Deviations of the pipe from being perfectly circular are corrected by measuring the maximum and minimum diameter. The average of the maximum and minimum diameters is taken as mean diameter and is further used in installation of the ultrasonic paths [5].

4.6 NUMERICAL INTEGRATION ERROR

One important source of error is the error in numerical integration used for discharge measurement from UTTF observations. More on the causes of the error and its significance in discharge measurement is discussed in the next Chapter.

The percentage contribution of error in discharge measurement due to the above mentioned sources of errors is tabulated as follows:

Table 4.1 Percentage error contribution of different sources of errors in discharge measurement

Roughness error for Ks=0.1	0.6 %
Protrusion effect for e/D =0.025	0.6 %
Roundness error for 1 % out of roundness	0.12%
Installation and survey errors	0.1 % - 0.2 %
Integration error (if corrected)	Can be restricted to 1%

One very important fact that needs to be realized is that all the sources of error influence the flow profile.

CHAPTER 5
NUMERICAL INTEGRATION METHODS

It is very explicit that most of the practical systems cannot be complete with respect to the mathematical modeling. Tools like differentiation and integration are indispensable in the practical applications. Functions (or outputs) in most cases are defined in tabular or graphical format which makes them difficult for differentiation and integration as elementary functions. The plausible solution in such situation is numerical integration. On the flip side application of numerical integration techniques to an application reduces that number of samples of the outputs that are to be obtained to preserve the required accuracy.

Though there can be many reasons why numerical integration methods are preferred, one reason is that it may be very difficult or impossible to find a mathematical function for integration to be carried out analytically. Another reason is that though a mathematical relation is obtained, it may be that there are no computation tools with such caliber to handle the function (in case the complexity of the function is high). Simple numerical integration methods are Simpson's $1/3^{rd}$ rule, trapezoidal rule, etc., whose formulation is independent of the application and thus giving enough chance to result in significant error. Applications demanding high accuracy certainly should be treated with special numerical integration techniques that suit them best. Discharge measurement using UTTF is one such complicated application.

5.1 GAUSSIAN QUADRATURE METHODS

The basic integration schemes use equally spaced sampling points. The accuracy of such numerical integration can be improved by splitting the range of the function into number of individual ranges, over which numerical integration is applied to obtain the required accuracy. This seems to be absurd when related with the practical application because, the basic objective of any measurement application is to optimize the number of output samples required for the demanded accuracy. Gaussian quadrature techniques are such methods which optimizes the sampling points and also the weighting factors. An

appreciable fact about the Gaussian quadrature technique (open quadrature formula) is that the function values need not be known at the end points, but must be known at predetermined sampling points.

Consider the formula:

$$\int_a^b f(x)dx = \sum_{1=0}^{n} a_i f(x_i) + E \tag{5.1}$$

where

f(x) is the a function,

$f(x_i)$ is the value of the function at abscissa x_i,

n is the number of sampling points,

a_i is the weighting factor corresponding to i^{th} abscissa and

E is the numerical integration error.

The interval from (a,b) is normalized to (-1,1) for simplicity in the calculation of unknowns (abscissae and weighting factors). Substituting function of degree 0 to (2n-1), we obtain (2n) conditions, which can be used to obtain the unknowns of polynomial of degree (2n-1). The number of unknowns is (2n), it is reasonable that the abscissae and weighting factors can be chosen so that any polynomial of degree (2n+1). For sure the error, E in (5.1) is equal to zero (for n point quadrature formula) for any function of degree (2n+1) [20, 21]. The error increases with the increase in the polynomial degree from (2n+1) and there after, if an n point quadrature formula is applied.

5.1.1 GAUSS-JACOBI (GJ) NUMERICAL INTEGRATION METHOD

Also called as the Tchebychev numerical integration method, this is one of the gaussian quadrature techniques used for the application of eight-path UTTF. From Table 2.1 it is clear that the shape factor for GJ, *k*, is equal to 1.000 for closed conduits and 0.994 for rectangular channels, indirectly suggesting that GJ is method that suits for closed pipes.

5.1.2 GAUSS-LEGENDRE (GL) NUMERICAL INTEGRATION METHOD

GL is no different from GJ, except that the abscissae and the weight are different. The shape factor from Table 2.1 can be seen as 1.0 for rectangular sections and 1.034 for closed pipes. So GJ can be a suggestive method for rectangular channels. The abscissae and the corresponding weights are listed in Table 5.1.

5.2 OPTIMAL WEIGHTED INTEGRATION FOR CLOSED SECTIONS (OWICS)

OWICS as mentioned in the previous chapter is introduced to take care of the installation error [18]. But as it can be seen that OWICS too uses the same abscissae as that of GJ, and the weights are optimized to these lateral distances. Due to the optimized weighting factors the numerical integration error is less than that of GJ. This is supported by the results presented in chapter 7. The weighting factors are reproduced here and these for the absicissae of GJ are listed in the Table 5.1

The weighting factors of OWICS are as follows:

$$\left.\begin{aligned}
W_1 &= \frac{g_1 D^2 (d_3 + d_4 - d_2) - g_2 d_2 d_3 d_4}{\left(1 - 4d_1^2/D^2\right)(d_1 - d_2)(d_1 + d_3)(d_1 + d_4)} \\
W_2 &= \frac{g_1 D^2 (d_3 + d_4 - d_1) - g_2 d_1 d_3 d_4}{\left(1 - 4d_2^2/D^2\right)(d_2 - d_1)(d_2 + d_3)(d_2 + d_4)} \\
W_3 &= \frac{g_1 D^2 (d_1 + d_2 - d_4) - g_2 d_1 d_2 d_4}{\left(1 - 4d_3^2/D^2\right)(d_3 - d_4)(d_1 + d_3)(d_2 + d_3)} \\
W_4 &= \frac{g_1 D^2 (d_1 + d_2 - d_3) - g_2 d_1 d_2 d_3}{\left(1 - 4d_4^2/D^2\right)(d_4 - d_3)(d_1 + d_4)(d_2 + d_4)}
\end{aligned}\right\} \quad (4.5)$$

where

d_i is the lateral distance of the i^{th} UTTF path from diameter,

D is the diameter of the pipe,

g_1 and g_2 are the constants and

W_i is the weight of the corresponding i^{th} UTTF path.

The abscissae and the weights of GJ, GL and OWICS are tabulated as follows:

Table 5.1 Abscissae and weights of GJ, GL and OWICS methods

	GJ		GL		OWICS	
	Paths 1 and 4	Paths 2 and 3	Paths 1 and 4	Paths 2 and 3	Paths 1 and 4	Paths 2 and 3
d/(D/2)	± 0.809017	± 0.309017	± 0.861136	± 0. 339981	± 0.809017	± 0.309017
W	0.369317	0.597667	0.347855	0.652145	0.365222	0.598640

5.3 ROLE OF NUMERICAL INTEGRATION IN DISCHARGE MEASUREMENT

Integration can be seen as a summation series with the number of sampling points in the given interval as infinity. Numerical integration can be treated as a simplified model of exact integration, owing to the constraints imposed by the complexity of the application and optimization tradeoff. A four point Gaussian integration technique is applied when measuring discharge with multi-path UTTF.

The eight-path UTTF uses four-point Gaussian quadrature technique. The two abscissae (n=4) are the lateral distances above and below the (horizontal) diameter. IEC 60041 ascertains that each of the paths in a plane (at an angle to the flow propagation) should be complimented by an axis-symmetric path in order that the transverse component of the low velocity cancels out. Thus the UTTF in the discussion comprises of eight paths.

The first step in flow rate measurement using multi-path UTTF is the installation of ultrasonic transducers at certain lateral distance from the diametrical path and at a certain angle with respect to the flow direction. The normalized lateral distances, as specified by IEC 60041, are $\pm$ 0.809017 and $\pm$ 0.309017, which have a six-digit resolution. This implies that it is very important to measure parameters like diameter, path length and angle with a similar resolution and accuracy. The calculation of flow rate (discharge) from the average velocities measured by UTTF along the eight paths should also have a matching accuracy.

An *n-point* gauss quadrature technique suits best to *n-path* UTTF. If compensation for transverse flow component is considered, it is applicable to a *2n-path* UTTF. Thus 18 path UTTF, with each path complimented by an axis-symmetric path, is supposed to use 9-point quadrature technique for discharge measurement. The weighting factors for the paths corresponding to symmetric position above and below diameter have the same weights. Thus the number of weights in actual is two for an eight path UTTF. This is due to the symmetric shape of the flow conduit in the closed pipe. These weights are given in the following table:

Table 5.2 weighting coefficients for discharge measurement in circular pipes

	Gauss-Legendre method	Gauss-Jacobi method
$W_1' = W_4'$	0.176841	0.217079
$W_2' = W_3^1$	0.613298	0.568320

Then the original equation used for discharge measurement will be as follows:

$$Q = \frac{D^2}{2} \sum_{i=1}^{n} W_i' \bar{v}_{ai}$$

where

$\bar{v}_{ai}$ is the average velocity measured by ith ultrasonic path,

W_i' is the weights taken from Table 5.2,

D is the diameter of the pipe and

Q is the discharge measured.

5.4 NUMERICAL INTEGRATION ERROR AND WHY ?

In the first place, it is to be remembered that the numerical integration treats the output required (discharge) as a polynomial of *fixed order*. But pipe flow analysis reveals that the flow distribution is not static, but dynamic in nature. The flow profile is very sensitive to the discontinuities and the roughness of the pipe which cannot be easily quantified. The assumption that flow profile is static contributes to error in discharge measurement. An LDA analysis show that the flow profile varies with the parameters of the pipe flow. The variation in the flow profile is directly reflected in the degree of the flow polynomial.

Thus change in the degree to a higher value demands a higher-point quadrature method to be used to preserve the accuracy.

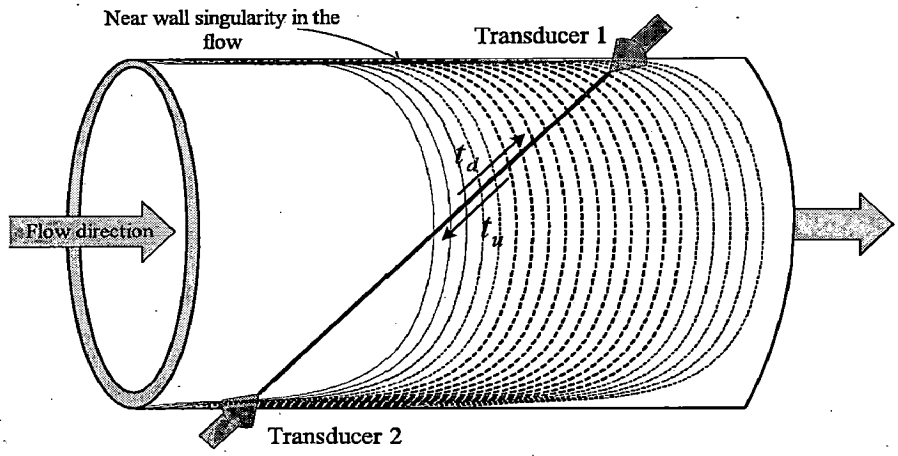

Fig. 5.1. Near-wall singularity in the flow conduit (side view of pipe).

While rapid variation in the flow profile is an important source for the numerical integration error, another cause that significantly effects numerical integration error is the near-wall flow. The near-wall flow complexity is discussed in detail in Chapter 3. The reason that hampers the performance of quadrature techniques is that the flow distributions near the wall. The flow distribution cuts deep along the wall with a steep descent, till the flow velocity near the pipe is nearly zero.

The quadrature techniques are best suited for smooth flow distributions with no singularities at any point of the flow profile. Singularity is an abrupt zero which changes the flow profile so much that it gets distorted. Obviously the numerical integration is not going to probe into that rapid variation in the profile, and takes it for granted that the profile is smooth with no singularities unless other wise the UTTF path cuts through such an abrupt variation. Whether there is a singularity in the flow profile function or not, but there exists always singularity near the pipe wall which is going to affect the accuracy of numerical integration, thus the numerical integration error is always in the place.

The near-wall flow pattern comprises of a steeply descending function. Such a steep function in the flow profile is responsible for a poor performance of numerical integration techniques and holds them back from being 'exact', especially in case of distorted flow. .

What Gauss was clever enough to realize ~~was~~ that by treating both n sample points and the n weights as variables, one should be able to make exact for polynomials of 2n coefficients. The idea behind Gaussian quadrature is that the abscissae (n in number) represent another n+1 degrees of freedom, which extended the exactness of the rule to polynomials of degree 2n+1

CHAPTER 6

DATABASE: ANALYTICAL FLOW PROFILES

Mathematical modeling of any system enables research to proceed comparatively at a higher pace. The analysis and prediction of the system thereafter becomes an easy task. Moreover the actual existence of the situation is not a necessary condition to study the cause and effect on the system for variation in different parameters. Such a modeling of the flow profiles into mathematical equations and their grouping is studied in this chapter.

6.1 MATHEMATICAL MODELLING OF FLOW DISTRIBUTION IN CLOSED PIPES

Though costly, experimentation to visualize the flow profile under different circumstances is to be done over the years, which resulted in mathematical modeling of the flow distribution, termed as 'flow profile'. Technologies like Doppler global velocimetry and laser Doppler anemometry or particle image velocimetry are used to investigate the flow in closed pipes efficiently. The generalization cannot be reached as such unless otherwise enough evidence for the statistical agreement of the experimental results under similar conditions. The reliability of the generalization of the flow profiles is dependent on the resolution with which the flow in the closed pipe is probed.

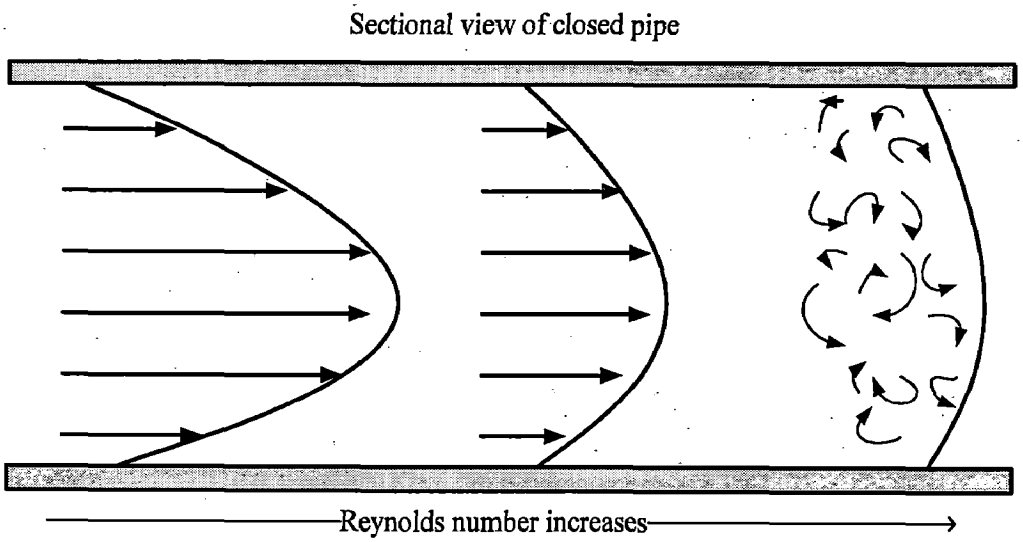

Fig 6.1. Flow profile variation with respect to the increase in R_e

Initially the flow profile definition is assumed to be parabola or a power law with an exponent 1/2. But sooner, experimentation revealed that flow profile is not always parabolic but only at low Reynolds numbers i.e., laminar flow. The index of the power law is not 1/2 two but ranged to the order of 1/9. An approximate variation in the flow profile as the Reynolds increases is shown in Fig. 6.1. An equation (6.1) defines the laminar and turbulent flow for different n in closed pipes.

$$\frac{V(r)}{V_{max}} = \left(\frac{R-r}{R}\right)^{1/n} \tag{6.1}$$

where

$V(r)$ is the flow velocity at a point r in the pipe,

V_{max} is the maximum velocity observed for particular profile,

R is the radius of the pipe and

n is the index for the kind of flow, where 2 corresponds to the laminar flow and 1/9 for a class of fully developed turbulent flow.

6.2 GROUPING OF FLOW PROFILES

The flow profiles are not one and the same even incase of similar field situations. The sensitivity of the flow profiles with various parameters at site is high. *Salami* was the first researcher to put forth the mathematical definitions of the flow profiles known as the analytical profiles [22]. The profiles are categorized into 3 major groups. Equation (6.2) gives the mathematical definitions for these categories. These definitions are intended for the flow profiles in closed pipes. The profiles focus on the distortion in the flow profile with respect to different parameters in the field.

$$V = (1-r)^{1/n} + mr(1-r)^{1/k} f(\theta) \tag{6.2a}$$

$$\left.\begin{aligned} V &= 1 + zr\sin\theta && \text{for } r \le b,\ 0 \le b \le 1 \\ V &= (1 - zb\sin\theta)\left(\frac{1-r}{1-b}\right)^{1/n} + m\frac{(r-b)(1-r)^{1/k}}{(1-b)^{1/k}} && \text{for } r \ge b \end{aligned}\right\} \tag{6.2b}$$

$$V = \sin\left(\frac{\pi}{2}(1-r)^{1/n}\right) + m\sin\left(\pi(1-r)^{1/k}\right) f(\theta) \tag{6.2c}$$

Equation (6.2a) shows that the velocity distribution is a function of both r and θ, and subject to the parameters n, m and k. The actual shape of the profile depends on these parameters, whereas the asymmetry of the profile is determined by the function $f(\theta)$. The topological parameters like that of single bend out of plane, double bend out of plane and inclination of the pipe prior to the measuring section are imbibed in $f(\theta)$. The parameters n, m and k are functions of Reynolds number, pipe roughness, transducer protrusion and other systematic parameters that affect the flow profile.

The analytical profiles eased the way of research in this field. The profiles could be simulated in the laboratory using advanced computing tools like CFD, Matlab and FLUENT, etc. This has enabled for the pre-analysis and prediction of the behavior of the flow profiles without actually realizing the flow profiles in field. But before going to take up further work on these profiles, one important question that needs to be answered is that whether these profiles match with the actual flow profiles in the

Table 6.1 Functional and parametric description of analytical profiles [26]

Profile Code†	n	k	m	a	$f(\theta)$
Single peaked profiles					
P6	9	4	$-\frac{0.5}{\pi}$	-	$\theta\sin\theta$
P17	7	9	$-\frac{0.4}{\pi}$	-	$\theta\sin\theta$
P8	9	4	$\frac{0.04}{\pi}$	-	$(\theta^2-1)(1-\cos\theta)^2$
P1	9	0.5	3.3170	0.5	$e^{-a\theta}\sin\theta$
P12	7	9	$\frac{e^{0.1\pi}}{2}$	0.2	$e^{-a\theta}\sin\theta$
P13	7	9	$-\frac{e^{0.1\pi}}{2}$	0.5	$e^{-a\theta}\sin\theta$
P9	9	4	$\frac{2}{\pi^5}$	-	$\theta^2(2\pi-\theta)^2$
Double peaked profiles					
P7	9	4	$\frac{1}{\pi^2}$	-	$\theta(1-\cos^2\theta)$
P10	9	4	$\frac{2}{\pi^3}$	-	$\theta(2\pi-\theta)\sin^2\theta$
P5	9	9	0.6813	0.1	$e^{-a\theta}\sin^2\theta$
P16	7	9	$e^{0.1\pi}$	0.2	$e^{-a\theta}\sin^2\theta$
Complex profiles					
P2	9	0.5	-6.7501	0.5	$e^{-a\theta}\sin\theta$
P22	7	9	$\frac{1}{2\pi^2}$	-	$(2\pi-\theta)^2\theta\sin 3\theta$
P20	4	9	$\frac{e^{0.15\pi}}{2}$	0.3	$e^{-a\theta}\sin^2 5\theta$
TU	9	represented as $(1-r)^{1/9}$			
LA	2	represented as $(1-(2r))^{1/2}$			

†.Salami's Profile code

field situations. The answer is a certain yes! The correlation between the analytical profiles and the actual field profiles is evident from the techniques such as laser Doppler anemometry [23-25].

The first category of flow profiles (14 in number) represented by (6.2a) is taken up for analysis and prediction of the discharge measurement using multi-path UTTF. Along with these fully developed turbulent flow and laminar flow, TU and LA respectively are included as ideal and uniform cases of flow. The equation for TU can be obtained from equation (6.1) by substituting n=9. TU is illustrated in Fig. 3.3. The 16 profiles in total are taken up for further study. The definitions for these 14 profiles are obtained from [26], which also presents the analysis of the performance different configurations of the UTTF with respect to the angle of installation. The definitions are reproduced in Table 6.1.

The three basic categories of the analytical profiles (equation 6.2) are in some way special cases of each other [25]. These 14 flow profiles seem to correlate with the site conditions of single and double out of the plane bends, which are generally found in hydro-power stations. The 14 profiles are divided into 3 classes, first 7 (P6 to P9) with a *single peak* in the profile, next 4 (P7-P16) with *double peak* and the last 3 (P2-P20) that neither belong to the first nor the second category and are declared as *complex* kind of profiles. More about the significance of the profiles and their constants for a particular profile is discussed in next chapter.

6.3 DISTORTED FLOW PROFILES AS SUPERIMPOSED FUNCTIONS

The property used in introducing distortion in flow profiles is superimposition of two functions. Superimposition of functions is combination or overlap of the functions in the same boundary specified. Eqn.(6.2a) can be re-written as (6.3). An almost ideal flow profile out of considerably straight conduit can be represented as the term FD in the profile [27]. Introduction of the second term of (6.3) will result in flow distortion or asymmetry in the flow profile.

$$V = FD + m\ SF = \{(\text{fully developed flow}) + m\ (\text{superimposed functions})\} \quad (6.3)$$

Fully developed flow is nothing but power law (eqn. 3.4), while the second term introduces distortion in the flow profile. And *m* is the factor that decides on the amount of distortion in the flow profile. Higher the value of the *m* higher the asymmetry in the flow profile surface. The variation of different profile parameters with respect to the site conditions is discussed in detail in Chapter 7. These definitions are visualized using Matlab 6.5 by the method of finite elements analysis. The visualization of 14 flow profiles is presented in Fig. 6.2. This gives better picture of how and why of the flow profile.

Analytical profiles enable behavioral study of different UTTF models since UTTF's principle of calculating the average flow rate along a path can be realized using profile expressions

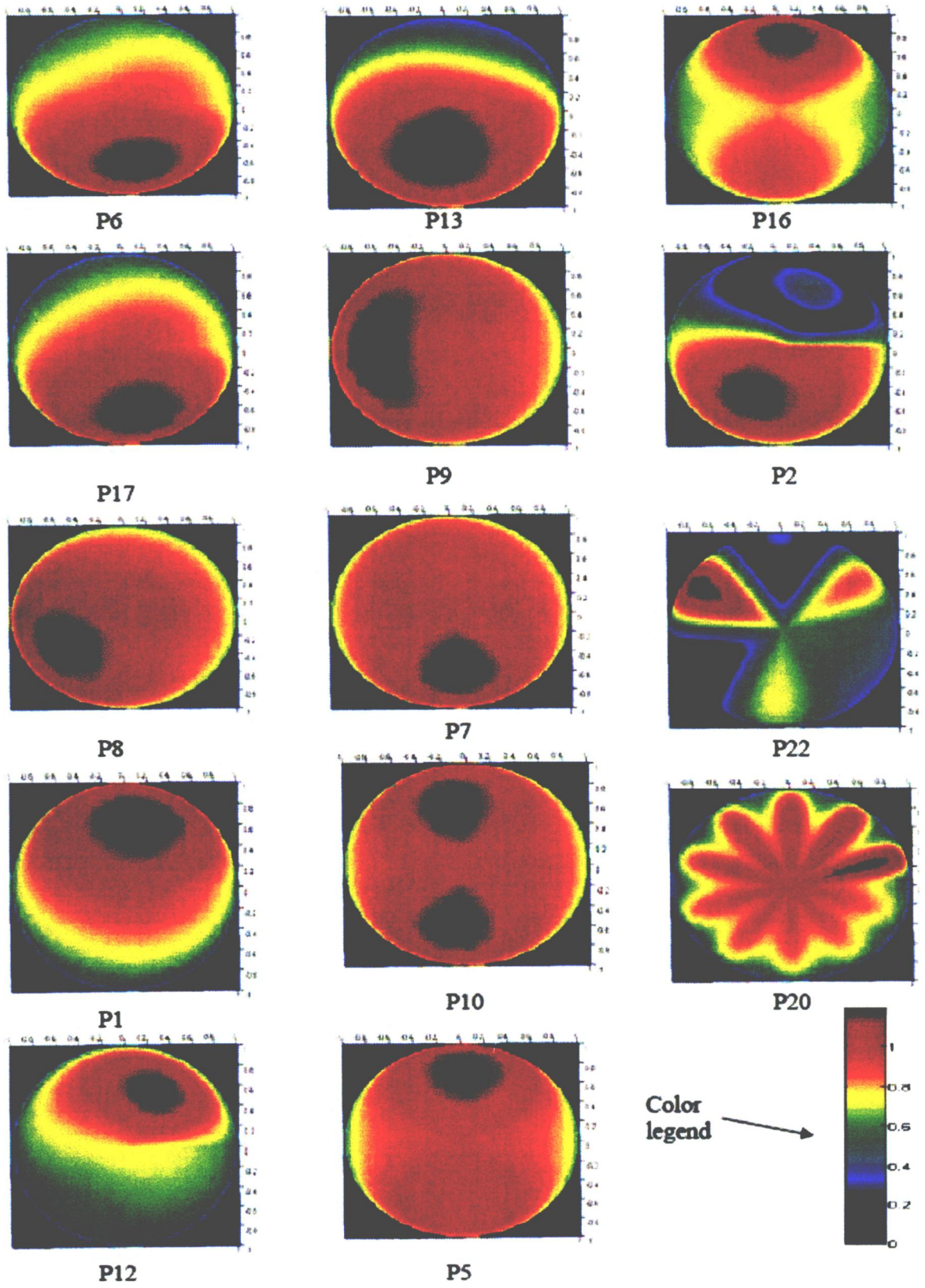

Fig 6.2 Visualizations of 14 profiles listed in Table 6.1.

CHAPTER 7

NUMERICAL INTEGRATION ERROR IN DISCHARGE CALCULATION

The analytical profiles provide a good ground for the pipe flow analysis. The profile expressions are used for the reason of being integrable functions. The UTTF's principle of discharge measurement is numerical integration of the average flow velocity values measured along the individual ultrasonic paths. The measurement of average flow velocity along an ultrasonic path can also be carried out with a finite element analysis of the flow profile using a suitable computational tool. This implies that innovative UTTF models can be put to behavioral study with respect to the flow profiles, thus giving a method of checking the performance of any UTTF model.

A multi-path UTTF provides sampled flow velocities of the whole flow distribution in a pipe. Owing to the complexity of the flow distribution a simple average of sampled flow velocities measured along the individual ultrasonic paths result in large errors. Gaussian quadrature techniques, which account for this kind of flow distribution in a pipe, are commonly applied. The abscissa of the Gaussian quadrature technique is the lateral distance along which an ultrasonic path is fixed. The number of paths is twice the number of abscissae at which the flow velocity is sampled. Increasing the number of abscissae will increase the number of paths and reduce the error in the integration, and thus the numerically integrated value will get closer to the 'exact' value.

This chapter deals with the use of 14 profiles presented in chapter 6 to compute the errors contributed by different numerical integration methods. The UTTF model recommended in IEC 60041 is taken up for this analysis (Fig. 2.3).

7.1 FINITE ELEMENT ANALYSIS OF FLOW PROFILE

The profile surface is divided into finite elements by changing the values of r and θ in steps. Fig. 7.1 illustrates the step values dr, $d\theta$ and dl for radius r, angle θ and length l, respectively. The finite element considered for the analysis is shown as S and 1 to 4 are the four horizontal planes. There are two paths along each plane as shown

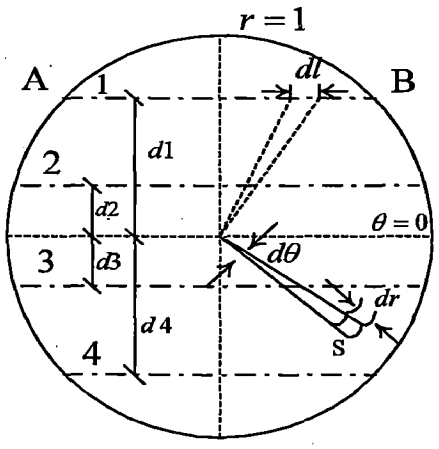

Fig. 7.1. Details of surface and path integration.

in Fig. 2.3. The analysis was carried out using *Matlab 6.5*. The surface and path integrals were computed using step sizes of 1/10, 1/100, 1/1000 and 1/10000, corresponding to 10^2, 10^4 ,10^6 and 10^8 finite elements of the total surface.

7.2 CALCULATION OF NUMERICAL INTEGRATION ERROR

The biggest advantage with the above flow profiles is that the exact value of discharge can be calculated from exact surface integration. The primary step in the analysis is to calculate the analogous value of discharge as measured by an eight path UTTF (Q_{MEAS}). Next, the actual discharge value against which the measured discharge has to be compared is calculated from surface integral (Q_{ACT}). Numerical integration error is difference between the measured and actual value of discharge expressed as the ratio of the actual discharge.

7.2.1 ACTUAL DISCHARGE CALCUALTION BY EXACT INTEGRATION

The mathematical profile expressions are used to find out the "actual" discharge with zero error. Exact surface integration is applied to the mathematical expressions of profiles to find out the actual value of discharge and in turn the mean velocity. Equation (7.1) gives the expression for the surface integration:

$$Q_{ACT} = \iint_S V_z(r,\theta)\, r.dr.d\theta \qquad (7.1)$$

where $V_z(r,\theta)$ is the velocity profile as a function of r and θ.

The parameters r and θ are varied from 0 to 1 and 0 to 2π, respectively. The actual mean velocity, V_{ACT} can be found from the following expression (r being 1):

$$V_{ACT} = \frac{Q_{ACT}}{\pi} \qquad (7.2)$$

7.2.2 DISCHARGE CALCUALTION BY NUMERICAL INTEGRATION

The same theoretical profiles are taken for evaluation of the three numerical integration techniques that are applied to multi-path UTTF, namely Gauss-Jacobi, Gauss-Legendre and OWICS. The individual path velocities are calculated and these are subjected to process of numerical integration to obtain the "measured" discharge using the following equation:

$$Q_{MEAS} = \sum_{i=1}^{n} W_i \cdot [V_{Path}]_i \qquad (7.3)$$

where $[V_{Path}]_i$ is average flow velocity along i^{th} ultrasonic path and Q_{MEAS} is the measured discharge calculated from numerical integration method. Further, the average velocity along an ultrasonic path is given by

$$V_{Path} = \frac{1}{L} \int_{\theta_1}^{\theta_2} V(\theta).\, d\theta \qquad (7.4)$$

where

$V(\theta)$ refers to the flow profile parameterized in θ,

L is the length of ultrasonic path, and

θ_1 and θ_2 are the limits for the ultrasonic path.

7.2.3 ERROR CALCULATION

The difference between the "actual" value and the "measured" value obtained from numerical integration is the error ascribed to the numerical integration technique. Thus it is given by

$$\% \ Error = \left[\frac{Q_{MEAS}}{Q_{ACT}} - 1 \right] \times 100 \tag{7.5}$$

7.3 FLOW CHART AND RESULTS

Figure 7.2 illustrates the steps followed in calculating the numerical integration error for the three numerical integration techniques namely Gauss-Jacobi, Gauss-Legendre and OWICS. The results are tabulated in table 7.2.

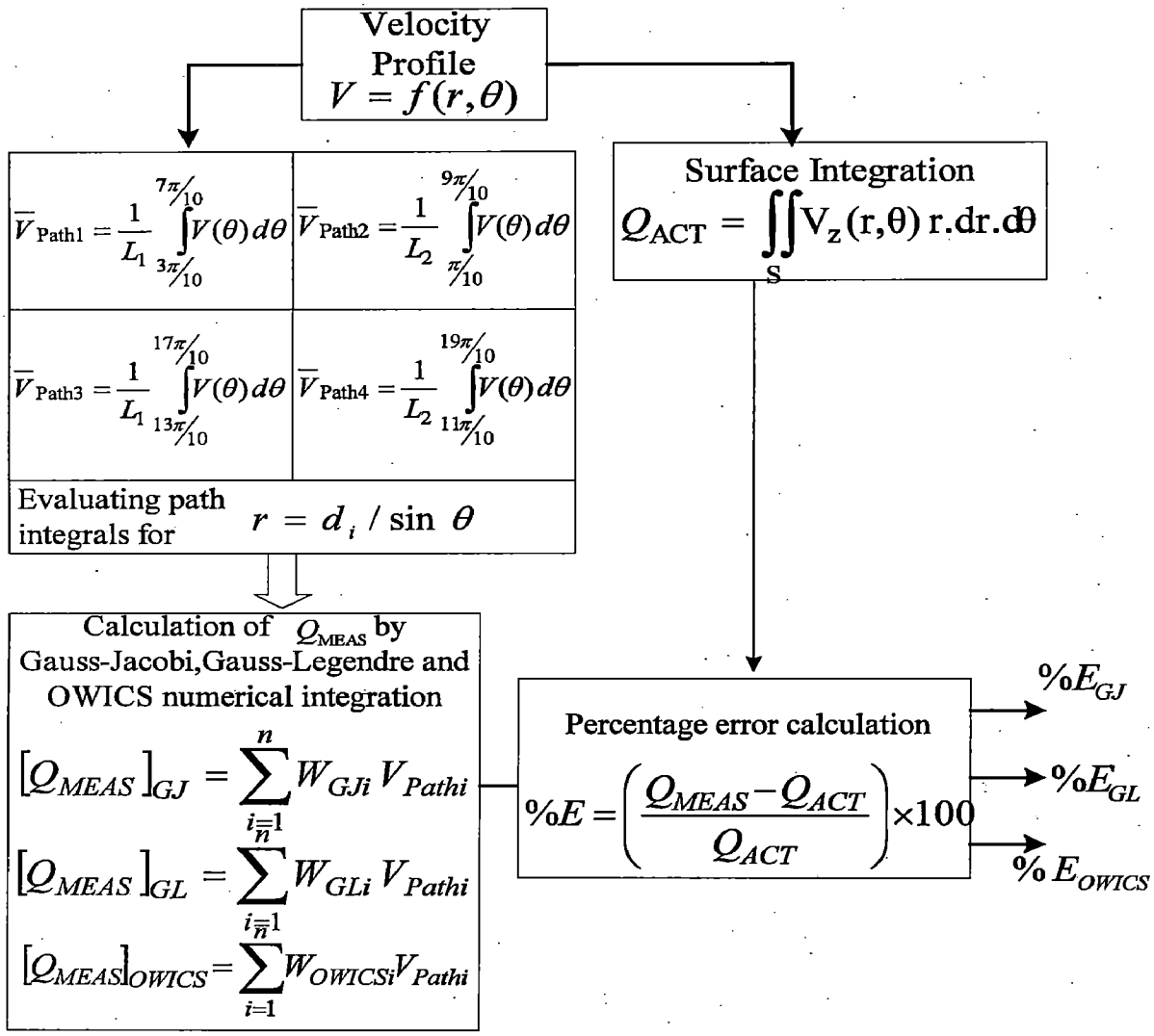

Fig. 7.2 Steps involved in the calculation of numerical integration error.

Table 7.2 Numerical integration error for Gauss-Jacobi, Gauss-Legendre and OWICS methods

S. No.	Profile Code	Q_{ACT}	Q_{MEAS}			Percentage Error		
			Q_{GJ}	Q_{GL}	Q_{OWICS}	E_{GJ}	E_{GL}	E_{OWICS}
1	TU	2.678593	2.680276	2.671957	2.676393	+0.062822	-0.247731	-0.082131
2	P6	2.897395	2.915162	2.909387	2.910404	+0.613210	+0.413874	+0.448997
3	P17	2.784857	2.800597	2.794216	2.796116	+0.565193	+0.336035	+0.404272
4	P8	2.932214	2.935210	2.925811	2.930930	+0.102156	-0.218359	-0.043810
5	P1	3.065476	3.103614	3.099145	3.098630	+1.244095	+1.098300	+1.081519
6	P12	2.694662	2.704812	2.696968	2.700742	+0.376649	+0.085588	+0.225638
7	P13	2.436562	2.430090	2.418066	2.427172	-0.265654	-0.759109	-0.385385
8	P9	3.145370	3.154204	3.145502	3.149207	+0.280846	+0.004171	+0.121970
9	P7	2.897395	2.908934	2.902689	2.903914	+0.398278	+0.182719	+0.225002
10	P10	2.992498	3.006535	3.000710	3.000954	+0.469083	+0.274413	+0.282563
11	P5	3.113029	3.129804	3.128254	3.123421	+0.538876	+0.489078	+0.333848
12	P16	3.230025	3.255318	3.255806	3.248017	+0.783050	+0.798152	+0.557006
13	P2	2.128007	1.998371	1.972909	1.995449	-6.091884	-7.288391	-6.229189
14	P22	2.699390	2.632726	2.632790	2.631361	+1.845992	+1.848463	+1.793175
15	P20	2.544042	2.589714	2.532190	2.586609	+1.795228	-0.465887	+1.673207
16	LA	1.141605	1.141013	1.158387	1.142838	-0.051794	+1.470933	+0.108075

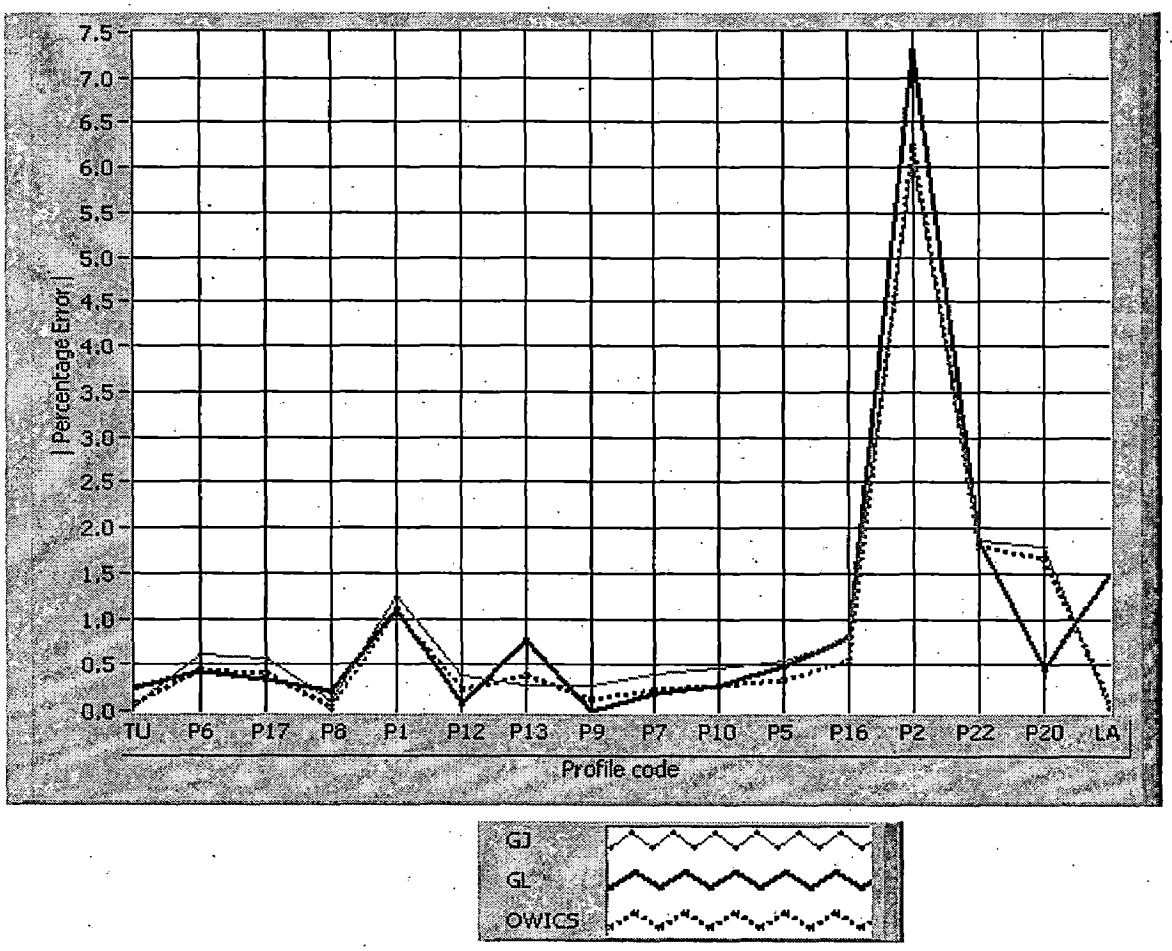

Fig. 7.3 Numerical integration error for different flow profiles and methods.

The results for numerical integration error by Gauss-Jacobi (GJ), Gauss-Legendre (GL) and OWICS methods are analyzed and the following interesting points are observed:

1. OWICS always performs better than GJ, the reason being that for the same lateral distances the weights of OWICS are derived by optimization for the actual lateral distances.
2. In most of the cases, OWICS gives better performance than even GL.
3. GL performs better than other two methods for profiles P20 and P9, which indicates that GL can do well for profiles resulting from one bend out of the plane.

4. For profiles P9 and P12 GL gives lowest errors but OWICS also performs well as it does for most of the profiles.
5. As observed from the results of P2, P22 and P20, OWICS performs better as in the periodicity of $f(\theta)$ increases. The ratio of 2π and the period of $f(\theta)$ is nothing but the number of bends in the proximity of the measuring section. So as the number of bends increases OWICS does better.
6. In the profiles where the value of '*m*' is very large, for example P1 and P2, the error is large for all the three methods.

The following section is completely devoted to quantify the parameters of the flow profile expressions with respect to the site conditions, the conclusions drawn are based on the profile visualization and analysis for numerical integration.

7.4 INTERPRETATION OF SITE PARAMETERS AND FLOW PROFILE PARAMETERS

A potential problem in the field of flow measurement is to correlate the parameters of mathematical profile expressions with the situations that exist on the hydro-power station. An attempt to probe into the influence of the site parameters on the flow profile is made here. Conclusions are reached by observing the behavior of profiles while the analysis for numerical integration error is carried out. For convenience the profile expression (6.2a) is reproduced below:

$$V = (1-r)^{1/n} + mr(1-r)^{1/k} f(\theta)$$

$$f(\theta) = e^{-a\theta}\varphi(\theta)$$

The parameters of involved say *n, k, m, a* and $f(\theta)$ are correlate to site parameters.

7.4.1 'n'

The value of n is function of Reynolds number, R_e of the flow and roughness of the pipe inner wall of the pipe, K_s. Its value observed in Table 6.1 comes out to be always in the range of 7 to 9. The quantification can be reached by carrying out the profile measurements and simultaneous measurements of Reynolds number and roughness of the

pipe inner wall. Relating them through an empirical relationship may not be complete, and could be very profile specific. As the value of n increases from 7 to 9, the turbulent core increases and the laminar sub-layer thickness decreases. Thus for higher values of n (without any distortion), the flow profile is closer to fully developed flow.

$$n = f(R_e, K_s, ...) \tag{7.6}$$

7.4.2 'k'

The significance of k is similar to that of n. It is also function of Reynolds number and roughness of the pipe. The values of taken in the 14 profiles are 4, 9 and 0.5, which decide the distortion distribution over the circular cross section.

$$k = f(R_e, K_s, ...) \tag{7.7}$$

7.4.3 'm'

The value of m decides the intensity of the effect of a given discontinuity in the penstock. The discontinuity may be a single bend out of plane, double bend out of plane or inclination in the proximity of the measuring section. A higher value of m indicates that the discontinuity in the penstock is closer to the measuring section and vice versa. The value of can be quantified as function of the distance between the measurement section and the discontinuity. The discontinuity may be upstream or downstream of the measuring section. The effect (value of m) is more incase of upstream discontinuity.

$$m = f(L_1, L_2, ...) \tag{7.8}$$

where L_i is the distance of i^{th} bend from the measuring section.

7.4.4 'a'

The value of a in the decaying exponential function is vital in deciding the rate of decay of the distortion with θ. It may be a function of the angle of inclination of the bend in the proximity of the measuring section. The sharper the bend the lesser the rate of decrease in the flow distortion as the profile is observed from 0 to 2π. In short the effect of sharper bend is that it would spread the distortion all over the profile. A low value of a, relates to a sharp bend and mathematically a slow decaying exponential. Smoother bends only

result in distorting the profile partially. Centrifugal laws of physics are valid for the travel of flow profile through a bend, which give better reasoning for the asymmetry in the profiles

$$a = f(\alpha, r_\alpha, \beta, r_\beta, ...) \tag{7.9}$$

where

α *and* β are the angles of curvature of the bends and

r_α *and* r_β are the radius of the curvatures of the bends.

7.4.5 'f(θ)'

f(θ) is a function of the number of bends and spatial orientation of one bend with respect to the other bend or with respect to the measuring section. A good observation that can be made from Table 6.1 is that the periodicity of the function has a direct linear relation with the number of bends in the proximity of the measuring section. The number of bends is the ratio of 2π to the periodicity of f(θ).

Fig 7.4 illustrates the relationships between the profile parameters and the site conditions.

Discharge measurement with UTTF has an important advantage if the above correlation is available in empirical terms. This makes the prediction of profile behavior ahead of measurement easier. Thus a correction factor corresponding to the various sources of errors would possibly be operated on the "as obtained" discharge value to calculate accurate discharge using less than eight ultrasonic paths.

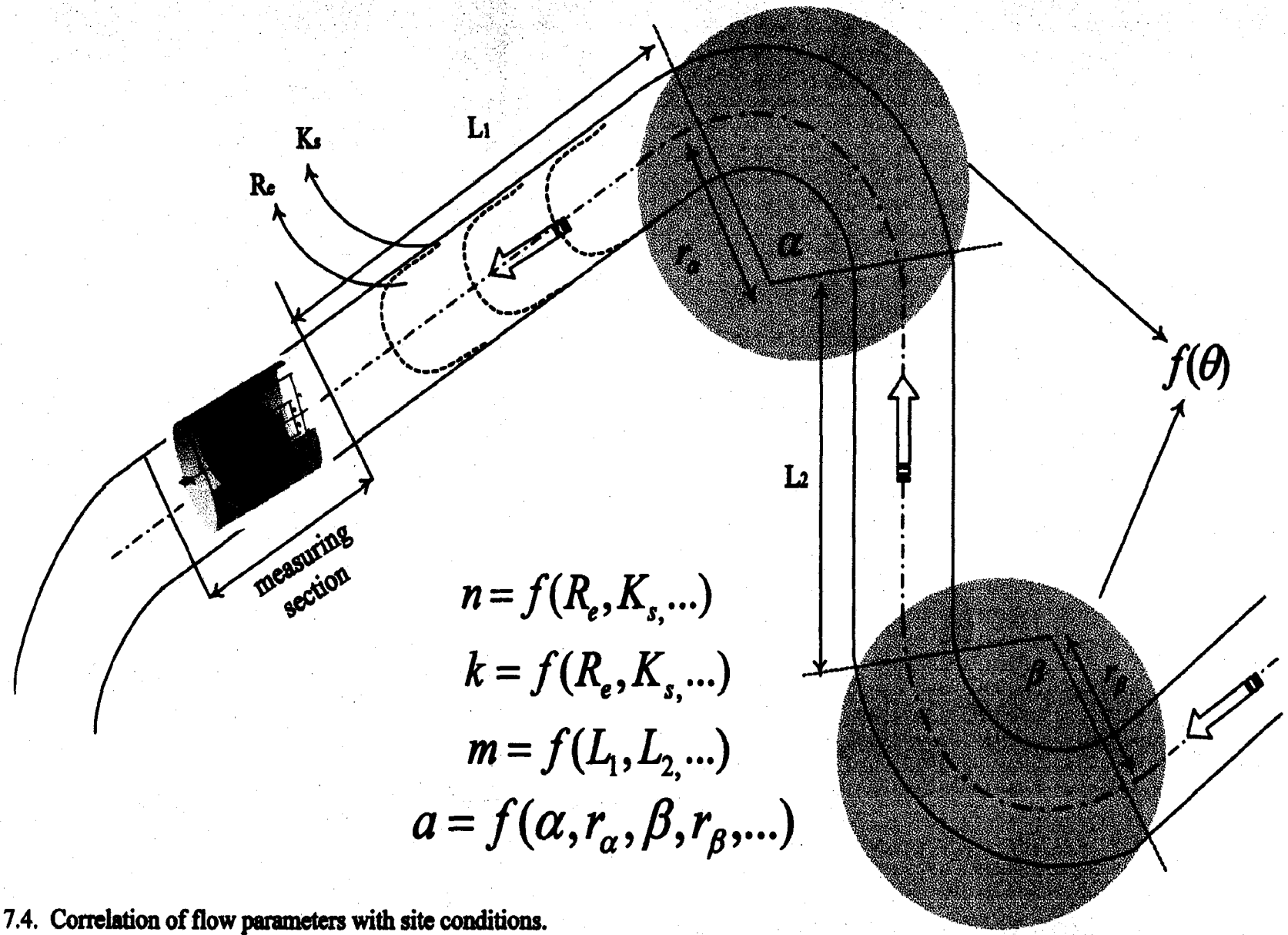

Fig. 7.4. Correlation of flow parameters with site conditions.

CHAPTER 8

DISCHARGE PREDICTION USING NEURO-FUZZY MODEL

Of late, the complexity of applications increased to such saturation levels that conventional mathematics is too simple to solve the related problems. The evolutionary techniques like fuzzy logic, *artificial neural networks* (ANN) and genetic algorithm are now used for solving complex problems that defy solution using conventional mathematics. Broadly speaking, fuzzy logic is used for decision making, ANN for pattern recognition and prediction, and genetic algorithm to solve optimization problems. This chapter describes how ANN can be used to predict discharge using back propagation neural network (BPNN) along with fuzzy logic.

8.1 ARTIFICIAL NEURAL NETWORKS

After modeling most of the systems that exist in this nature, man started to explore himself. Attempts to model human brain led to break-throughs in computational techniques. As electron formed the fundamental element of the whole system, the human brain too is driven by a fundamental unit called biological *neuron* [28]. Neuron forms an essential entity in the architecture of the ANN.

Neuron can be imagined as a tiny system with incredible computing capability complimented by accurate sensing ability and interconnected with other neurons by high speed communication network. The biological structure and functioning of neuron can be found in [28]. The biological structure consists of *dendrites* which act as inputs due to their sensing action. The sensed inputs are weighed and carried to the *synaptic junction* attached to the body of the neuron. All such inputs reaching the neuron are summed to result in a single value. Now this value is given to the *soma*, which actually performs the thinking. The soma is termed as *excitation function* in mathematical terms. The amount of the *soma* and the ability to spread itself all over the body of the neuron to learn is a measure of the thinking capability of the neuron. The soma or neurotransmitter fluid contributes to the learning process of the brain. The biological structure and the corresponding mathematical structure are shown Fig. 8.1.

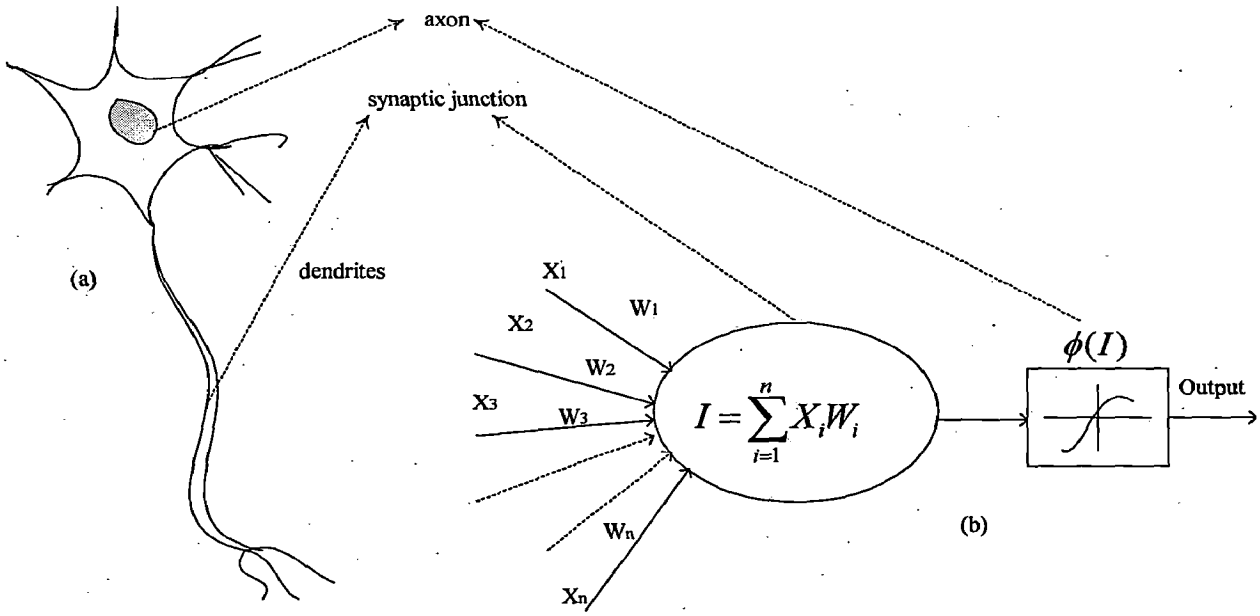

Fig 8.1. (a) Biological and (b) Mathematical structure of neuron.

The basic structure of neuron consists of number of input paths which sense. The sensed input values are sent to the body of the neuron via weighing factors. The summation over all the paths is taken and applied to an activation function inside the neuron. The function is the area where thinking is done. This is how neuron *learns* about the situation through inputs and *thinks* by itself.

Such neurons which are efficient computational units are interconnected on the scale of millions inside the human brain. A network of large number of neurons which communicate through a highly sophisticated interconnections is called ANN. ANN in short is simulation of human brain. The properties of ANN are similar to those properties of the neuron. The network learns from the past experience and recognizes or may predict for a new situation with very small or no error. An important thinking function is the sigmoid function or the logistic function which spreads over the large domain of the function thus helping the network to learn quicker, while it searches an N-dimensional plane for the *global minima* (with respect to error) without falling into *local minima.* N is the total number of weights used in the ANN. Mathematicly,

$$\left.\begin{aligned}\phi(I) &= \frac{1}{\left(1+e^{-\alpha I}\right)} \\ \frac{\partial \Phi(I)}{\partial I} &= \alpha(1-\Phi)\Phi\end{aligned}\right\} \tag{8.1}$$

where α is the sensitivity of the activation function $\phi(I)$

ANN is not a programmed structure but is a trained network which learns from example input-output patterns. Fig. 8.2 shows the structure of ANN. The network consists of the input, hidden and output layers of neurons, of which are interconnected with each other. A *feed forward path* is the path that proceeds from the input to error. One traversal of the feed forward path is called an *epoch*. In Fig. 8.2, I, H and O are the number of neurons in the input, hidden and output layers, X_i is the number of inputs, W_{ih} is the weight matrix relating input layer and the hidden layer, W_{ho} is the weight matrix relating hidden layer and the output layer, $I_h = X_i W_{ih}$ (matrix multiplication), $I_o = \phi_h(I_h) W_{ho}$ (matrix multiplication), $\phi_h(I_h)$ is the activation function, T_o is the target matrix corresponding to the input training pattern and E_o is the error matrix between the outputs of neural network and the targets.

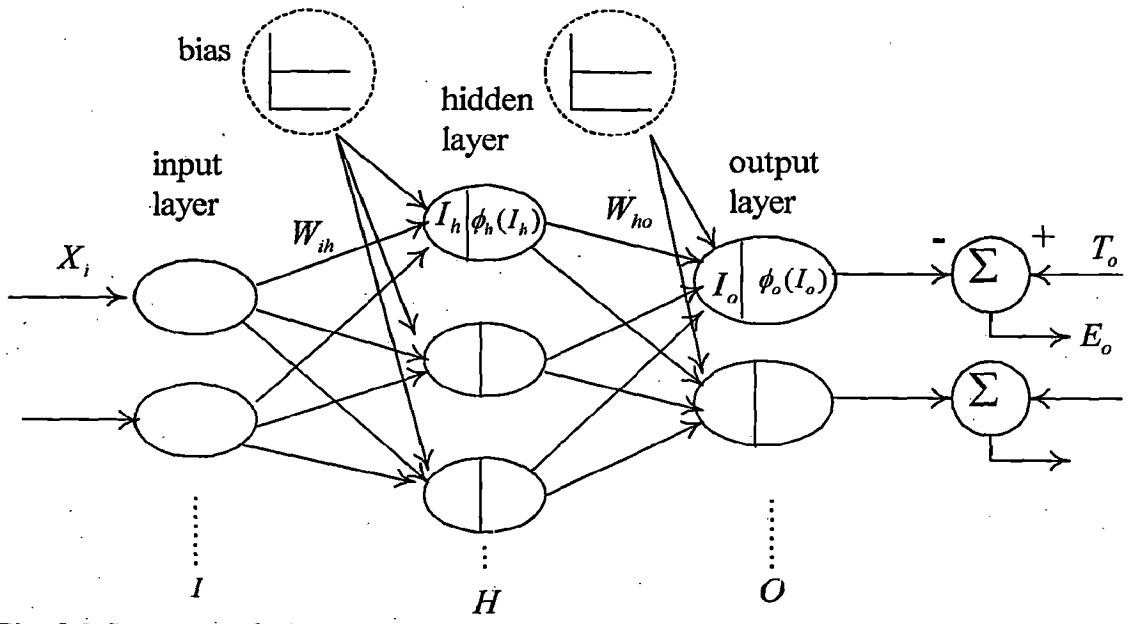

Fig. 8.2 Structure of ANN.

8.2 BACK PROPAGATION NEURAL NETWORK

The basic objective of to update the weights such that the error is minimized. Among different networks that are available, back propagation neural network (BPNN) is a highly successful and popular technique for pattern recognition. Its basic principle on which BPNN works is that the error calculated is fed back to the network as a root squared error. The weight matrices are updated according to the error. This is carried out for each of the input-output patterns that are available, and is repeated till the error reduces to less than a given threshold value (as demanded by the application). This process is called *training* and the input-output patterns used are called the *training patterns*. The mathematical expressions that BPNN uses in updating weights are below:

Error calculation:

$$E_o = [T_o - \Phi_o] \tag{8.2}$$

Weight upgradation of output neurons:

$$\left.\begin{aligned} \delta_{ho} &= \frac{\partial \varepsilon_o^{\,2}}{\partial W_{ho}} = \frac{\partial \varepsilon_o^{\,2}}{\partial \Phi_o}\frac{\partial \Phi_o}{\partial I_o}\frac{\partial I_o}{\partial W_{ho}} \\ W_{ho}(N+1) &= W_{ho}(N) + \eta \delta_{ho} \Phi_h \end{aligned}\right\} \tag{8.3}$$

Weight upgradation of hidden neurons:

$$\left.\begin{aligned} \delta_{ih} &= \frac{\partial \varepsilon_o^{\,2}}{\partial W_{ih}} = \sum \frac{\partial \varepsilon_o^{\,2}}{\partial \Phi_o}\frac{\partial \Phi_o}{\partial I_o}\frac{\partial I_o}{\partial \Phi_h}\frac{\partial \Phi_h}{\partial I_h}\frac{\partial I_h}{\partial W_{ih}} \\ W_{ih}(N+1) &= W_{ih}(N) + \eta\, X_i \sum_{q=1}^{o} \delta_{hq} \end{aligned}\right\} \tag{8.4}$$

where

δ_{ho} is the error of back propagation for updating hidden-output weights,

δ_{ih} is the error of back propagation for updating input-hidden weights,

η is learning rate,

W(N) is the weight to be updated and

W(N+1) is the updated weight.

The upgradation of weights is carried out through the training process till the error reduces to a minimum value. After the training phase is completed the accuracy of ANN

is checked for validation set (like the training set the validation set is a set of input-output patterns). If the accuracy is satisfactory, the network is used for testing where new input patterns are given and the pattern recognized or the predicted value is taken as the accurate output. Better picture of the process can be seen in Fig. 8.3.

8.3 NEURO-FUZZY MODEL FOR DISCHARGE PREDICTION

BPNN works effectively for the pattern recognition, especially when discrete targets are used. In order that prediction be made possible, fuzzy functions are added. The overall block diagram of the prediction model using ANN extended by adding fuzzy functions, is illustrated in Fig. 8.3. The three phases of modeling, namely training, validation and the testing are dealt with in detail below:

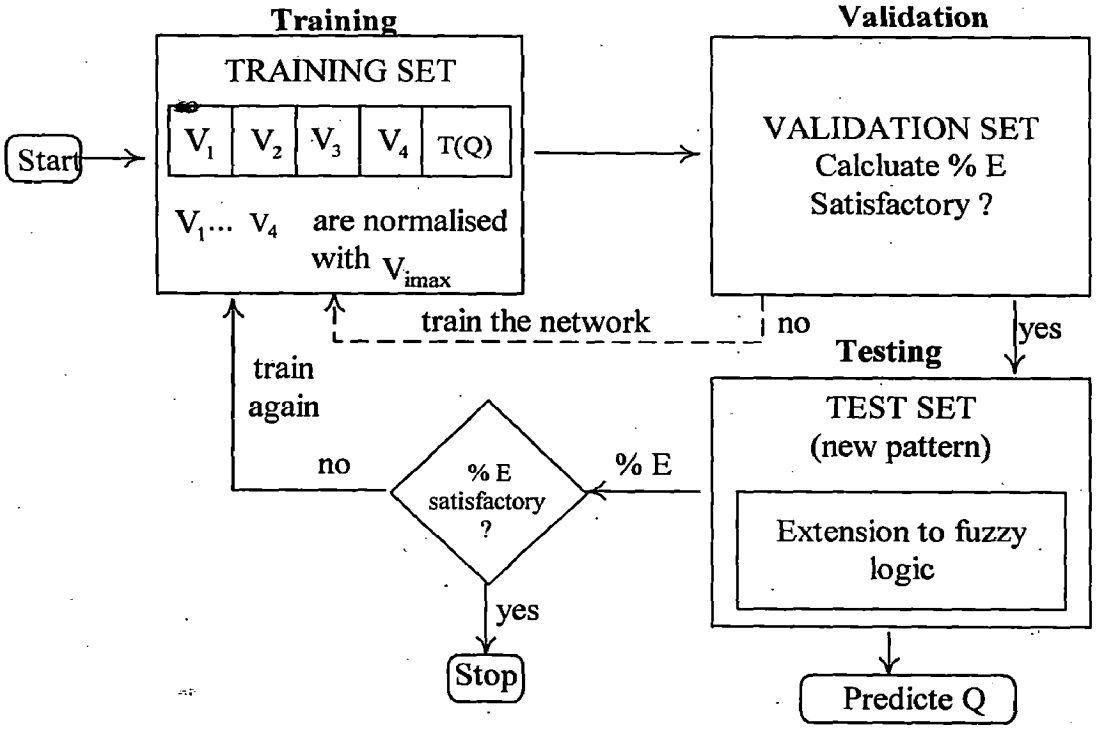

Fig. 8.3. Neuro-fuzzy model for discharge prediction.

8.3.1 TRAINING

BPNN requires training patterns for that define the relationship between the inputs and output. Moreover, the more the complexity of the relationship more is the requirement of input-output patterns. The training patterns used here have their origin in the profile

expressions discussed in chapter 6. Since these 14 profile expressions specify different classes of profiles, 14 training patterns are generated from them. The important point to be noted is that there is no transverse flow component in the profiles. Thus an 8-path UTTF can be seen to record equal path velocities for the two axis-symmetric paths in a plane or the path velocities of the axis-symmetric paths calculated from the profile expressions would be equal. So the eight path velocities reduce to the four distinct path velocities (each of the four distinct paths can be thought of as the average of the two path velocities measured by UTTF in that plane). These 4 path velocities and the actual discharge are calculated from equations (7.4) and (7.1), which is reproduced here for convenience.

$$V_{Path} = \frac{1}{L}\int_{\theta_1}^{\theta_2} V(\theta).d\theta$$

$$Q_{ACT} = \iint_{S} V_z(r,\theta)\, r.dr.d\theta$$

Table 8.1 Training sets corresponding to 14 profiles

S.No	Profile code	V_1	V_2	V_3	V_4	Q_{ACT}
1	P2	0.206116	0.296502	1.000000	0.942313	2.128007
2	P13	0.441322	0.770612	1.000000	0.962917	2.436562
3	P20	0.807915	1.000000	0.895060	0.693841	2.544042
4	P22	0.140529	1.000000	0.472800	0.703401	2.585007
5	P12	1.000000	0.953816	0.749296	0.534952	2.694662
6	P17	0.543353	0.724760	0.922769	1.000000	2.784857
7	P6	0.587794	0.731775	0.941729	1.000000	2.897395
8	P7	0.859453	0.920126	0.968591	1.000000	2.897395
9	P8	0.794512	0.932341	1.000000	0.914361	2.932214
10	P10	1.000000	0.965743	0.965743	1.000000	2.992498
11	P1	1.000000	0.995698	0.683149	0.576227	3.065476
12	P5	1.000000	0.876193	0.852563	0.917670	3.113029
13	P9	0.930838	1.000000	1.000000	0.930838	3.145370
14	P16	1.000000	0.779558	0.719083	0.790974	3.230025

Each training set comprises of 5 elements. 4 path velocities and actual discharge. Fourteen such training patterns have been formulated using *Matlab 6.5* and are tabulated in Table 8.1 in ascending order of actual discharge values. Note that the path velocities listed in Table 8.1 are the *normalized* values. The four paths are normalized using maximum of the 4 path velocities thus making the patterns suitable for the use of sigmoid function.

The number of input neurons is obviously 4, corresponding to the 4 ultrasonic path velocities. The number of neurons in the hidden layer is a judicious decision. By running the BPNN algorithm, it was found that the time of convergence to a threshold error is optimum in the range of 8-12 hidden neurons in the hidden layer. However 8 hidden neurons are used in the training and the phases thereafter to minimize the computational delay, incase the algorithm is applied in a real time system. The number of output neurons is equal to 6. This is based on the fact that the targets for which the BPNN is trained are discrete values (precisely binary digits). It clearly established from the following discussion that increasing the number of output neurons would increase the sensitivity of the network.

The slope of activation function α is set to 0.5. The learning rate η to 0.7 and the momentum value μ to 0.4. The parameters of the ANN are arrived at more by trial and error than by methodical ways. Moreover the method of arriving at the parameters of ANN is not established but an idea of cause and effect of different parameters on the ANN's functioning is obvious. The discharge values for 14 profiles are assigned to different binary targets (output neurons) depending on the separation of one from the other, as they are arranged in ascending order. So the profile with least and maximum values of discharge will have binary targets close to 000000 and 111111, respectively. Thus using the resolution provided by the 6 output neurons is used to the fullest.

The training is done for as good as approximately 10,000 iterations and the validation and testing phases are carried out to check whether the discharge is predicted within 0.5 % accuracy. The training-validation-testing process is repeated till the criteria on accuracy

is met with. The error which the converged ANN reaches least effects the accuracy of the ANN to perform the pattern recognition.

8.3.2 VALIDATION

The process of validation is similar to training except that the weights are not upgraded, but used for verification of the network accuracy in identifying different profiles. A few training profiles are taken up each time after training the network and applied to the network for validation. The network is checked for its accuracy. If not satisfactory then the training process is repeated with new ANN parameters and the process is continued till all the profiles in the training set are accurately identified by ANN. The validation process is decision making phase as of when the network is ready for use.

The ANN under discussion was finally observed to be performing with zero error for all the known profiles. Thus the network is validated for all these profiles.

8.3.3 TESTING

The testing phase is similar to but the validation with the difference being that the new patterns that are given to the ANN. These new patterns may be similar to or may substantially differ from the training patterns. The testing phase is divided into two sections, namely recognition and prediction.

8.3.3.1 RECOGNITION

Recognition is one thing that ANN promises. The recognition process by which ANN works is by watching the *trend* in the inputs. The 14 profiles for which the network is trained are flawlessly recognized as expected. More profiles were generated by changing the amount of distortion in the profile (value of m) and or the values of n and k, such profiles were also recognized without any error.

The recognition process can be explained as a way of watching the fired (output=1) neurons. Since targets are digitized, the change of misidentification is almost eliminated. The binary targets assigned to the profiles and their discharges in ascending order are

listed in Table 8.2. The training process is carried out till the sigmoid function value of the corresponding output neurons is almost unity, leaving difference between the digitized and the saturated value of the output neuron to the order of 10^{-3}. The network is observed to be precise in profile identification.

Table 8.2 Binary targets assigned to profiles

Profile code	Binary targets	Actual discharge value, Q_{ACT}
P2	000100	2.128007
P13	001000	2.436562
P20	001100	2.544042
P22	010000	2.585007
P12	010100	2.694662
P17	011000	2.784857
P6	011100	2.897395
P7	100000	2.897395
P8	100100	2.932214
P10	101000	2.992498
P1	101100	3.065476
P5	110000	3.113029
P9	110100	3.145370
P16	111000	3.230025

8.3.3.2 PREDICTION

Prediction is the output of the neuro-fuzzy model for a new input profile pattern. The number of profiles used for training is just 14. The demand is of the order 7-10 for each of the weights in the ANN, which means nearly 800 patterns. Generating patterns in such numbers is a tedious process and more over the accuracy will be dependent on the deviation in the actual discharge for each of the generated patterns from the 14 profile classes. An alternative method of handling all the missing profiles is used here, which consists in adding fuzzy logic.

Another important reason why the prediction was taken up as part of the improvement is that the path velocities in the field never completely match with the path velocities of the trained profiles. There might be variation in the normalized path velocities in the 4^{th} or 5^{th} place of the decimal point in the best case. This suggests us that it is also important to predict discharge value corresponding to the new path velocities.

Fuzzy logic as the name suggests helps us to express a crisp number into a fuzzy function and vice versa. The processes are called *fuzzification* and *defuzzification*. The neuro-fuzzy model proposed for the present application is shown in Fig. 8.4. A matrix of the saturated values for all the 14 profiles is data-logged in the beginning of the testing phase. For a new pattern (new profile close to any of the 14 classes), the discharge is predicted as function of the deviation of the new profile from the known profile. The deviation is obtained as defuzzified value of the error as ratio to the equivalent decimal weight corresponding to the bit position of the binary target. The fuzzy function can be expressed as the following equation:

$$f(\delta E_i) = \left(\frac{2^i}{E_{Th}}\right)\delta E_i \tag{8.5}$$

where

δE_i is the deviation of the i^{th} bit value of the binary target from that of the profile class identified,

E_{Th} is the threshold value of the error at the end of training phase and

$f(\delta E_i)$ is the fuzzy function defined for the calculation of the deviation.

As suggested by above equation, the fuzzy function used is a triangular function. The value obtained from the equation (8.5) for each of the output neurons is summed and divided by the maximum value of the binary targets to obtain the accumulative error as a fraction.

$$\Delta E_D = \left[\frac{\sum_{i=1}^{k} f(\delta E_i)}{2^k}\right] \tag{8.6}$$

where

ΔE_D is the cumulative of the error

k is the number of output neurons or the number of bits in the binary target (k=6 in fig. 8.4).

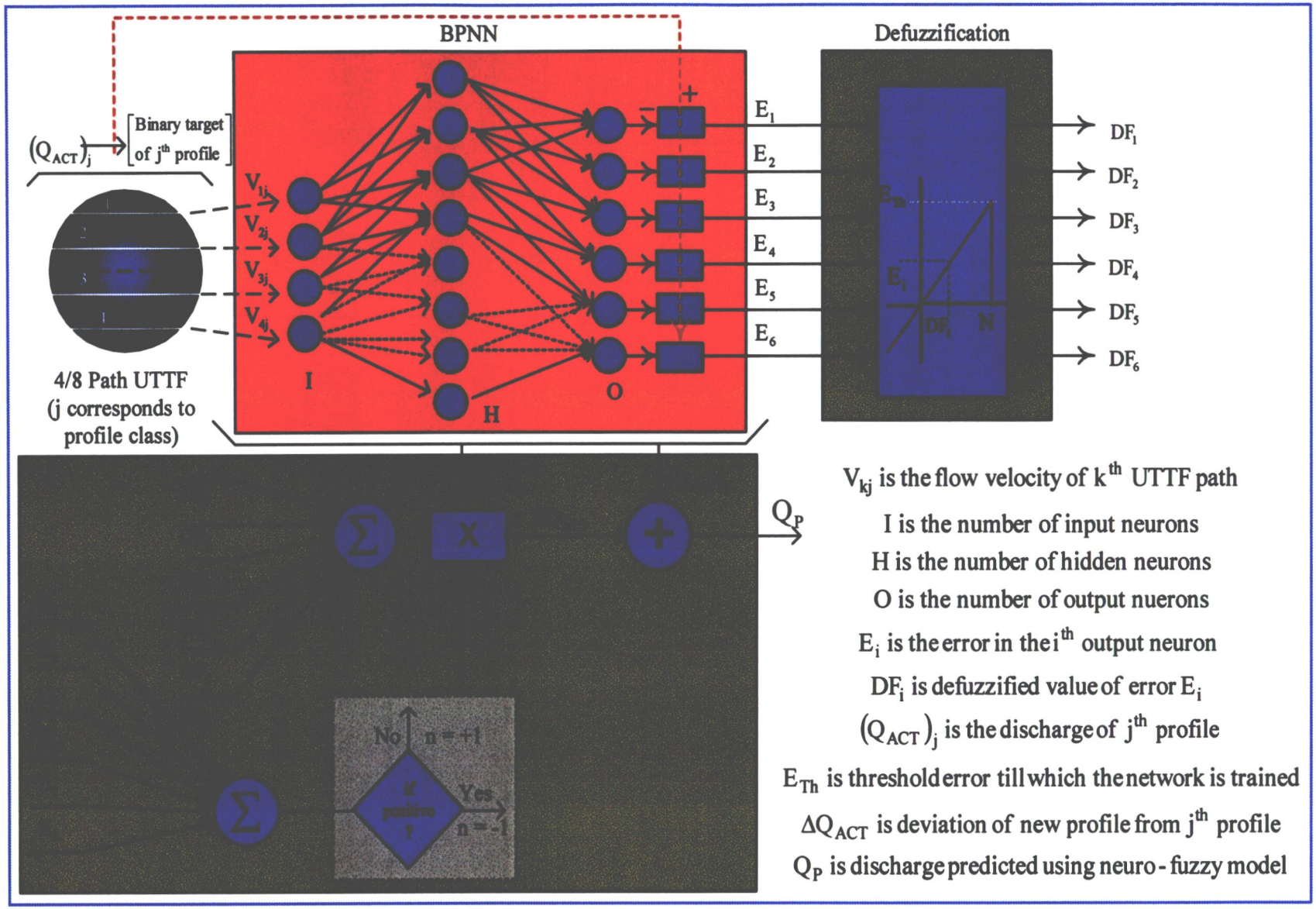

Fig. 8.4 Neuro-fuzzy model for profile recognition and discharge prediction

The next step is to calculate the deviation in the discharge corresponding to the deviation calculated from Eq. (8.6). The following expression gives the deviation in the discharge.

$$\Delta Q_p = \Delta E_D . (Q_{ACT})_j \quad (8.7)$$

where

$(Q_{ACT})_j$ is the actual discharge of the j^{th} profile identified and

ΔQ_p is the deviation of the new profile's discharge from the actual discharge of identified class.

The next step is to add or subtract the value of ΔQ_p from the actual discharge to predict discharge. The discharge predicted can be calculated from the following expression:

$$Q_p = (Q_{ACT})_j + n.\Delta Q_p \quad (8.8)$$

where

$n = +1$, if $\sum_{i=1}^{k} \delta E_i < 0$, else n= -1,(where k is the number of output neurons).

8.4 TEST RESULTS

The neuro-fuzzy model for profile identification and discharge prediction is tested for different input patterns and the accuracy of the model is assessed. From Table 7.2 it is clear that profiles P20, P22 and P2 result in large numerical integration error in increasing order. Along with these, worst classes, profiles P6 (single peaked – single bend out of plane) and P7 (double peaked – double bend out of plane) are tested on the model. The results are tabulated in Table 8.3. It can be seen that the profile identification is correct and the discharge predicted is equal to the actual discharge with zero error.

The next phase of testing was done using new patterns generated by varying the parameters of the known profiles. Profile P6, P1 and P7 are chosen as they seem to be out of single and double bends respectively. The test results are presented in the Table 8.4. The predicted discharge value is compared against the actual discharge calculated from the exact surface integration (equation 7.1).

Table 8.3 Test results of neuro-fuzzy model for input patterns from training set.

S.No	Path velocities (as input patterns to ANN)				Profile identified	Q_P	% Error in discharge predicted
	V_1	V_2	V_3	V_4			
1	0.807915	1.000000	0.895060	0.693841	P20	2.544042	Zero
2	0.140529	1.000000	0.472800	0.703401	P22	2.585007	
3	0.206116	0.296502	1.000000	0.942313	P2	2.128007	
4	0.587794	0.731775	0.941729	1.000000	P6	2.897395	
5	0.859453	0.920126	0.968591	1.000000	P7	2.897395	

Table 8.4 Test results of neuro-fuzzy model for new input patterns generated (outside the training set).

S.No	Path velocities (as input patterns to ANN)				Q_P	Q_{ACT}	% Error in discharge predicted
	V_1	V_2	V_3	V_4			
1	0.613191	0.762721	0.959740	1.00000	2.851633	2.858775	-0.1547
	+5 % in *m* for profile P6						
2	0.584073	0.733410	0.945260	1.000000	2.894270	2.876011	+0.6349
	-5 % in *n* for profile P6						
3	0.595821	0.738834	0.947886	1.000000	2.892989	2.881133	-0.4098
	-5% in *k* for profile P6						
4	0.790720	0.929370	1.000000	0.915830	2.932157	2.944895	-0.4325
	+5 % in *m* for profile P1						
5	0.848590	0.903501	0.955711	1.000000	2.790053	2.919275	-4.4265
	+10 % in *m* for profile P7						
6	0.852784	0.914648	0.965412	1.000000	2.895670	2.895737	+0.0023
	-3 % in *n* and + 5% in *m* for profile P7						

A close examination of the above results leads to the following inferences:

(i) For the same percentage change in *m*, *n* and *k*, the error in predicted discharge is more significant for the change in *n* and *k*.

(ii) For all profiles, the error in predicted discharge increases with the change in the value of *m*. Possibly, 10 % variation in *m*, is the worst case that can be found in the field.

(ii) For small variations in the site parameters (which in turn bring about small changes in profile parameters) the neuro-fuzzy model works very well for all profiles within 0.5 %.

If limited to the class of profiles on which the neuro-fuzzy model is trained, the error in the discharge predicted is very small. Each profile of the same class is unique by itself, yet the model identifies the pattern accurately and predicts discharge with a very satisfactory accuracy. The proposed neuro-fuzzy model thus holds a high promise for field application.

The neuro-fuzzy model proposed here has capability to significantly improve the accuracy of the UTTF for discharge measurement.

CHAPTER 9

CONCLUSION AND FUTURE SCOPE

9.1 CONCLUSION

In spite of the fact that ultrasonic transit time flow meter uses the state of art technologies, the discharge measurement is not free from error. The numerical integration error influences the accuracy of discharge measurement significantly. The improvement exercise first demanded an in-depth analysis of numerical integration error with respect to the method of integration and the parameters of the flow profile. Analysis using finite-element techniques gave an insight into the various aspects of the problem. One among them is the correlation of the profile parameters with respect to the site conditions. An attempt had been made to quantify these correlations into empirical relations, however it seems that such an analysis may never be complete and evaluating the correction factors will be a very tedious and time consuming task.

A finite-element analysis on the 14 of standard profiles has been carried out on Matlab 6.5. These profiles have also been used as the database in framing the training patterns for neuro-fuzzy model of the eight-path ultrasonic of flow meter. The model is novel in nature and gives significant improvement in the accuracy of discharge measurement. However, the model can work accurately for the class of profiles used to train the back propagation neural network. For the profiles belonging to or close to the 14 standard classes of profiles used for training, the error is almost completely eliminated. But for other similar profiles the error is restricted to 0.5 %. Under any circumstances, the neuro-fuzzy model proposed here is found out to be highly accurate for profile recognition.

9.2 FUTURE SCOPE

Scope of research as an extension to the work done here is very wide. A few suggestions are given below:

(i) The remaining profiles proposed by Salami [22, 25] of the other two classes can be taken up by the similar kinds of analysis.

(ii) The finite element analysis can be made rather than Matlab, as the former would allow insight into the variations of the flow profile with change in the diameter of the pipe and protrusion.

(iii) The fuzzy extension of the back propagation network can be further investigated with other than the triangular function which is used here.

(iv) The back propagation neural network is highly successful model for pattern recognition, but for the problems such as discharge measurement using ultrasonic transit time flow meter more complex models of neural networks, which consists of more hidden layers may work more efficiently.

(v) The neuro-fuzzy model can be realized on FPGA using hardware description languages like VHDL or verilog.

(vi) The fluid mechanics perspective of the problem suggests that more analysis of the laminar sub-layer can be carried out to arrive at some conclusions related to the fully developed flow for high Reynolds numbers.

(vii) Experimental verification of the established flow profiles with respect to the variation in the site conditions is of course a huge task. Quantification of the correlation factors involved is a big challenge.

(viii) This work is focused on the closed pipes. Carrying out similar kind of analysis and developing a model that can improve the accuracy of discharge measurement in open channels will be equally useful.

REFERENCES

[1] IEC-60041, Field acceptance tests to determine the hydraulic performance of hydraulic turbines, storage pumps and pump turbines, 1991.

[2] *The Measurement, Instrument and Sensors*, CRC press, John G Webster, 1999, pp (28-74) – (28-89).

[3] Edward J Thompson, "Mid-radius Ultrasonic Flow Measurement", *Flow measurement of Fluids*, North-Holland publishing company, 1978.

[4] Spitzer D W, *Flow Measurement*, The instrumentation, systems, and Automation Society, chap. 20.

[5] Voser A, Bruttin Ch, Pretnat J.-E. and Staubli T, "Improving Acoustic Flow Measurement", *Water Power and Dam Construction*, April 1996.

[6] Technical data sheets of Ryttimeyer for Risonic 2000.

[7] Reynolds O, "An experimental investigation of the circumstances which determine whether the motion of water shall be direct or sinuous, and of the law resistance in parallel conduits", *Phil. Trans. Roy. Soc.* **174**, 935, 1884.

[8] Webber N. B. (1965). Fluid Mechanics for Civil Engineers, E. & F. N. SPON Ltd.

[9] Colebrook C. F and White C M, "Experiments with Fluid Friction in Roughened Pipes", *Proc. Roy. Soc. Series A*, **161**, 367, 1937.

[10] Colebrook C F, "Turbulent Flow in Pipes, with Particular Reference to the Transition region between the smooth and Rough Pipe Laws", *J. Inst. C. E.*, **11**, 133, 1938-39.

[11] John Laufer, "The structure of Turbulence in Fully Developed flow", NACA Report 1174, 1952.

[12] Kritz, J, "An Ultrasonic Flowmeter for liquids", *Proc. ISA*, 1955.

[13] Birger, G I , " Certain Problems in Calibrating Ultrasonic Flowmeters", *Izmerital naya Technika*, 1962, pp. 53-55.

[14] Russell G J and Sheldon L H, "Determining the Net Head Available to the Turbine", U.S. department of Energy.

[15] Anastasia Gribik, Queenelle Ogirri, Sara M Royce and Earl Osman P.Solis, "Flow in Pipes", 2002.

[16] Elling Sletfjerding and Jon Steinar Gudmundsson, "Friction Factor Directly From Roughness Measurements", *Trans. of ASME,* **125**, June,2003.

[17] Voser A, Entiwicklung and Einsatz eines 3D- Theodaliten-Messsystems in Wasserkraftanlagen, wasser, energie, luft 1/2, 1995.

[18] Alexandre Voser and Staubli T, "Integration Error of Multipath Acoustic Discharge Measurements in Closed Conduits", *IGHEM,* Reno, 1998.

[19] Alex Voser, "CFD-Calculations of the Protrusion effect and Impact on the acoustic discharge measurement accuracy", *IGHEM,* Montreal, 1996.

[20] Rajeshekaran S (1999), "Numerical Integration Methods in Science and Engineering", Wheeler publishing, pp 375-430.

[21] Gordan K. Smyth, "Numerical Integration", May 1997.

[22] Salami L A, "On velocity-area methods for asymmetric profiles", *University of Southampton Interim Report* V, 1972.

[23] Walus S., "The use of the ultrasonic flowmeter in the conditions other than normal", *FLOMEKO* ed H S Stephens *et al* (University of Melbourne) pp 171–6,1985.

[24] Frank S, Heilmann C and Siekmann H E 1996 Point-velocity methods for flow-rate measurements in asymmetric pipe flow *Flow Meas. Instrum.* **7**, 201–9.

[25] Salami L A, "Errors in the velocity-area method of measuring asymmetric flows in circular pipes", *Universityof Southampton Interim Report* I, 1971.

[26] Pamela I Moore, George J Brown and Brian P Stimpson , "Ultrasonic transit-time flowmeters modelled with theoretical velocity profiles ", Meas. Sci. Technol., Oct, 2000.

[27] Pedro I. Espina, T. T. Yeh, and Peter I. Rothfleisch and Stephen A. Osella, "Tele-Metrology and Advanced Ultrasonic Flow Metering", *FLOMEKO,* 2000.

[28] Laurene Fausett, Fundamentals of Neural Networks, 2nd Edition, 2004.